The Pennsylvania State University

The Graduate School

College of Engineering

THE USE AND OPTIMIZATION OF STAINLESS STEEL MESH CATHODES IN MICROBIAL ELECTROLYSIS CELLS

A Thesis in

Environmental Engineering

by

Yimin Zhang

Submitted in Partial Fulfillment
of the Requirements
for the Degree of

Master of Science

August 2010

The thesis of Yimin Zhang was reviewed and approved* by the following:

Bruce E. Logan
Kappe Professor of Environmental Engineering
Thesis Advisor

John M. Regan
Associate Professor of Environmental Engineering

Michael Janik
Assistant Professor of Chemical Engineering

Stephanie Velegol
Instructor of Environmental Engineering

Peggy Johnson
Professor of Civil Engineering
Head of the Department of Civil and Environmental Engineering

*Signatures are on file in the Graduate School

ABSTRACT

Microbial electrolysis cells (MECs) provide an efficient method to produce hydrogen from renewable biomass and wastewater. To develop a low-cost and highly efficient cathode remains a great challenge to the technology advancement. Based on the factor that stainless steel is much cheaper than platinum as catalyst, stainless steel mesh with higher surface areas than flat sheets were studied for the first time as cathodes in MECs. Current distribution analysis during hydrogen production, at different bubble coverage conditions, was used to evaluate the optimum wire thickness and pore size. Analysis of the electrochemically active surface area by cyclic voltammetry showed that mesh could have up to three times the active surface area of a flat sheet. The relative ranking of mesh in terms of current densities in MECs was in agreement with linear voltammetry studies at small bubble coverage. An optimal voltage of 0.9 V was demonstrated in respect to high hydrogen recovery (98 ± 4%) and overall energy efficiency (74 ± 4%). Hydrogen was produced at 2.1 ± 0.3 m^3H_2/m^3d (current density of 188 ± 19 A/m^3, 0.9 V applied) using the best SS mesh (#60) that had a relatively thick wire size (0.02 cm) and medium pore size (0.02 cm), with a specific surface area of 66 m^2/m^3. The use of the SS (stainless steel) mesh cathodes shows great promise for the development of low cost reactors. Novel designs using heat-treated carbon mesh as anode and SS mesh as cathode cost only 3 to 5% of the traditional materials consisting of carbon cloth, platinum, and binders.

TABLE OF CONTENTS

LIST OF FIGURES vi

LIST OF TABLES ii

ACKNOWLEDGEMENTS iii

Chapter 1 Introduction 1

Chapter 2 Literature Review 5

Chapter 3 Material and Methods 10

- 3.1 Cathodes 10
- 3.2 Electrochemical Analysis 11
- 3.3 MEC Reactor Construction and Operation. 12
  - 3.3.1 Single-cell Cubic Reactor 12
  - 3.3.2 Bottle Reactor 14
- 3.4 Gas Analysis 15
- 3.5 Calculations 16
  - 3.5.1 Hydrogen Yield and Production Rate 16
  - 3.5.2 Energy Recovery 17

Chapter 4 Results 20

- 4.1 Evaluation of Mesh Type 20
- 4.2 Mesh Characteristics 21
- 4.3 Hydrogen Evolution Rate Using Different Size Mesh 22
- 4.4 Current Densities and Maximum Hydrogen Production Rates in MECs. 26
- 4.5 Cathode Potential 29
- 4.6 Hydrogen Recovery 31
- 4.7 Comparison of Hydrogen Recovery with and without Methane Production 33
- 4.8 Electrical Energy Efficiency and Overall Energy Recoveries 34
- 4.9 Corrosion 35
- 4.10 Use of SS mesh as Cathode and Carbon Mesh as Anode in a Bottle MEC 37

Chapter 5 Discussion 39

- 5.1 Effect of Mesh Characteristic on Hydrogen Evolution Rate 39
- 5.2 Limiting Factor on Current Generation 41
- 5.3 Efficiency 42
- 5.4 Outlook for Using SS Mesh as a Cathode 42

Chapter 6 Conclusions 44

Chapter 7 Future Work 45

Appendix A Mesh Surface Area Calculation Example 46

Appendix B LSV Scan Results for Different Size Mesh 48

Appendix C Original 3D Graph of Current Distribution 50

REFERENCES 52

LIST OF FIGURES

Figure 2-1: A General layout of a MEC in which in the anodic compartment the bacteria can bring about oxidative conversions while in the cathodic compartment reductive process produce hydrogen. (26) 5

Figure 3-1: Types of SS 304 mesh used in studies: (A) and (C) are woven mesh, (B) and (D) are expanded mesh. (A) and (B) are 7 cm^2 round shape mesh, (C) and (D) are microscopic photos at 4 × magnification. 10

Figure 3-2: MEC reactor with an 8 cm gas collection tube, a stainless steel mesh cathode (left, the cathode was bent to have an opening at the top) and an ammonia-treated brush anode (right) 13

Figure 3-3: Schematic of sandwich-type electrodes in different configurations. 15

Figure 4-1: LSV curves for the SS 304 woven mesh #44, expanded mesh, flat SS and platinum carbon-cloth. 21

Figure 4-2: Hydrogen bubble visualization on SS mesh at 5 mA (A), 40 mA (B), 80 mA (C) 24

Figure 4-3: Current magnitude distribution versus mesh wire diameter and pore size at low current (A), medium current (B) and large current (C) 25

Figure 4-4: Current as a function of applied potential in cubic single cell MEC for flat SS and SS mesh #60 cathodes. 26

Figure 4-5: Current as a function of cathode and anode potential in cubic single cell MEC for flat SS and SS mesh #60 cathodes. 27

Figure 4-6: Volumetric current densities, Iv, comparison as a function of applied voltage for SS mesh #44, #60 and #165 cathodes. 28

Figure 4-7: LSV curves for different mesh cathodes tested in MECs (cathode voltage is versus SHE). Three lines in each linear current range were to show the hydrogen bubble effect which will be analyzed in discussion part 3.5.1. 29

Figure 4-8: Cathode potential (versus Ag/AgCl) versus time using flat SS and SS mesh cathodes at E_{ap} = 1.2 V, 0.9 V and 0.6 V. 30

Figure 4-9: Coulombic efficiency, cathodic hydrogen recovery efficiecy and overall hydrogen efficiency as a function of applied voltage for flat SS (A) and SS mesh #60 (B). 31

Figure 4-10: Hydrogen (solid line), methane (dash line) volume at each applied voltage for flat SS (square symbol) and SS mesh #60 (round shape symbol). 32

Figure 4-11**:** Gas composition for MECs with flat SS and mesh # 60 cathodes using old anode with methane existence and new anode adding BES at E_{ap} = 0.6 V. Error bar of MECs with used anode are based on duplicate measurements, error bar of MECs with new anode are based on three consecutive batch cycles.).....33

Figure 4-12: Cathodic hydrogen recovery as a function of applied voltage for flat SS and SS mesh #60 cathodes with used anode (open symbols) and new anodes after adding BES (filled symbols).....34

Figure 4-13: Total gas and current production versus time with SS mesh #60 cathode at E_{ap} = 0.9 V.....35

Figure 4-14: SEM image of SS mesh #60 before (A and C) and after 20 day use (B and D) as cathode in MEC. (A) and (B) are at 5 × magnification and (C) and (D) are at 1,000 × magnification.....36

Figure 4-15: Current output for bottle MECs with different electrode constructions.....37

Figure A-1: SS 304 woven mesh configuration, where *n* is mesh size, *d* is wire diameter and *b* is pore size.....46

Figure B-1: Examples of three time LSV scans for flat SS and mesh#42.....48

Figure B-2: Currents of different SS mesh at different cathode potential.....49

Figure C-1: Original current magnitude distribution in a three-dimensional space at low current (A), medium current (B) and large current (C).....51

LIST OF TABLES

Table 3-1: SS meshes characteristics used in LSV and current magnitude distribution analysis. 11

Table 4-1: Evaluation of different catalyst in terms of minimum required voltage (V_e) and slope of the applied voltage (V_h). 21

Table 4-2: Areas based on mesh properties and electrochemically active areas measured by CV. 22

Table 4-3: Correlation factors between current and SS mesh number, wire diameter, pore size, calculated surface area and measured electrochemical active area. 23

Table 4-4: Volumetric current density I_v and maximum hydrogen production rate Q of different meshes at different applied voltage. 28

Table 4-5: Comparison of meshes in terms of minimum required voltage (V_e) by LSV and cathode potential in MECs at different applied voltage. 30

Table 4-6: Summary of MEC hydrogen recovery and COD removal for different mesh cathodes. 32

Table 4-7: Summary of MEC energy efficiencies for different mesh cathodes. 34

Table 4-8: Metal composition of SS mesh #60 by SEM-EDS before and after 1 month of use in MEC as cathode. Table 3-9: Metal composition of SS mesh #60 by SEM-EDS before and after 1 month of use in MEC as cathode. 36

Table 4-9: Comparison of the maximum volumetric current densities and superficial current densities for two types of electrode construction in different reactors. 38

Table 5-1: Slope of the applied voltage (V_h) in low, medium and high current range (shown in Figure 3-9) for different meshes. 40

Table 5-2: Slope of the cathode voltage (V_h) of flat SS and SS meshes in different linear current range in MECs. 41

Table B-1: Current taken from LSV results (Figure B-2) of different SS mesh at different cathode potential (vs. SHE) 49

ACKNOWLEDGEMENTS

First and foremost, I am heartily thankful to my supervisor, Dr. Bruce E. Logan, whose encouragement, guidance and support from the initial to the final level made my graduate studies possible. One simply could not wish for a better or friendlier supervisor. I also thank Dr. Jay Regan, Dr. Michael Janik and Dr. Stephanie Velegol for accepting to serve on my committee.

I am indebted to all researchers in Dr. Logan's lab for helping me in my studies and research. In particular, I want to thank Dr. Shaoan Cheng for his support in a number of ways, Dr. Matthew D. Merrill for guiding me through electrochemical system and introducing me to the MATLAB programmer, Xin Wang for his direction in cyclic voltammetry analysis, and David Jones for constant technical support.

It is an honor for me to associate with many talented young peers here. To Fang Zhang, I am thankful for always helping me with my course work. Thank to Geoff Rader and Jack Ambler for their help on gas analysis. Thank to Hengjing Yan and Roland Cusick for their encouragement.

Many thanks go to my beloved families for their understanding and endless love, through the duration of my studies.

Chapter 1

Introduction

Fossil fuels including oil, coal and natural gas together supply 85 percent of the world's energy usage in 2008 (1, 2). According to the oil market report from International Energy Agency (IEA), “Global oil product demand is expected to rise by a robust 2.5% to 88.2 mb/d in 2008” The large demand has come closer than ever to exceeding the world’s known production capacity. If oil production remains constant until it's gone, it is estimated that there is enough to last 42 years. Similarly, there is enough natural gas to last 61 years, and enough coal to last 133 years (3). Nearly everyone realizes fossil fuel will become scarce and expensive within the life times of living humans.

In addition to the petroleum crisis, increased consumption of fossil fuels will yield an increased production of carbon dioxide, the main green house gas. Scientists are concerned that increasing concentrations of greenhouse gases in the atmosphere are causing a rise in global temperatures, with potentially harmful consequences for the environment and human health. Inevitably, a transition to sustainable energy sources is forthcoming. Alternative energy sources are renewable, including wind, solar, geothermal, hydroelectric, and biomass. Compared to conventional energy sources, they all have lower carbon emissions. Until now, only hydroelectricity and nuclear power have been significant alternatives to fossil fuel (1).

Hydrogen is the most abundant element on earth, and exists in inexhaustible quantities. Hydrogen gas has one of the highest energy density values per unit mass at 120 to 142 MJ/kg (depending on the heat of combustion). Currently, many people advocate a hydrogen economy, which is based on using hydrogen as an energy carrier. A hydrogen fuel cell simply combines hydrogen and oxygen chemically to produce electricity, water, and waste heat (4) and therefore it

is non-polluting to the environment. Fuel cells are more expensive to produce than common internal combustion engines, but they are becoming cheaper as new technologies and production systems develop.

Hydrogen gas can be produced in several different ways from hydrogen-containing compounds such as water, biomass, and fossil fuel. Currently, commercial bulk hydrogen is produced from nonrenewable natural gas (5) by steam reforming. Renewable methods for sustainable hydrogen production include water electrolysis and biological processes such as biophotolysis, photo- or dark-fermentation (6, 7). Only 4% of hydrogen is generated from water splitting using electricity gained from a variety of sources (8-11) at a typical energy efficiency of 56-73% (11). The efficiency of biophotolysis conducted by algae and photosynthetic bacteria is low and requires large surface area for the process (12). Hydrogen can be produced from various types of biomass including carbohydrates, such as glucose, and polysaccharides, cellulose by biological fermentation. However, fermentation yields are low, varying from 0.57–2.2 mol H_2/mol hexose, with an upper theoretical upper limit of 4 mol H_2/mol hexose despite a stoichiometric potential of 12 mol H_2 / mol hexose (13). The fermentation process leaves many end-products (for example, acetic acid, butyric acid and ethanol (14-16)), which can not be converted to hydrogen gas without an external energy input.

Recently, a new process to produce hydrogen from various organic substrate called electrohydrogenesis (17) was discovered. In a microbial electrolysis cell (MEC), bacteria on the anode oxidize the organic matter and convert energy, available in a bio-convertible substrate, into electricity. Using this process, combined with a small electrical input (0.14 V vs. 1.23 V needed for water electrolysis) (11, 18), the hydrogen is formed on an anaerobic cathode, usually with the help of a catalyst.

The advantages of this biocatalyzed electrolysis to produce hydrogen from waste biomass sources over conventional technology are multifold. Firstly, the reduced electricity consumption

could be as low as 0.6 kwh/m^3 H_2 using Liu et al.'s (17) approach (assuming an overall added potential of 0.25 V), which is much lower than the typical energy requirement of 4.5–5 kwh/m^3 for water electrolysis (19). The efficiency of a single-chamber membraneless MEC in Call et al.'s study (20), relative to the electrical input, reached over 400%. Second, no precious metals were needed on the anode because of self-sustaining microbial biocatalysts. Third, hydrogen can be recovered from the end products of fermentation, obtaining greater overall hydrogen yield in a fermentation system coupled with biocatalyzed electrohydrogenesis system than a fermentation system alone. In addition, the higher purity (100% in theory) of the produced hydrogen is another advantage compared to other biohydrogen production methods from organic materials containing biogases mixture (e.g., CH_4, CO_2, H_2S, NH_3, etc.) and thus expensive gas purification is not necessary (21, 22).

Although many advancements in MEC performance have been made, developing a cost-effective, scalable design is the most critical challenge for the MEC to become a mature hydrogen production technology (23). Rozendal et al. (24) determined that the cathode (including catalyst) accounted for the greatest percentage (47%) of the total capital costs for MECs. It has been proven that MEC can produce hydrogen with cost-effective high surface area stainless steel brush at similar hydrogen production rate and efficiencies with platinum-catalyzed carbon cloth cathodes (25), indicating that high cost precious metal catalysts are not needed. However, bubble entrapment and complex construction of MECs with using SS brush cathodes could limit the application of this approach. Also, the system will require careful design to avoid short circuiting due to the bristles of the brush touching the anode.

SS mesh that is flat can allow closer electrode spacing of the cathode to the anode, and it can have a higher surface area than a flat sheet lacking pores. The main objective of this thesis was to determine the characteristics of the best SS mesh in terms of hydrogen evolution rate in single-chamber membraneless MECs. Given that there is a wide choice of mesh depending on

mesh number, wire thickness, and pore size, linear voltammetry was conducted in an electrochemical cell to better select the optimum mesh size in terms of currents produced and bubble coverage. In addition to considering mesh size, electrochemically active surface areas measured by cyclic voltammetry provided an approach to determine the influence of these factors on current generation. The performance of mesh cathodes were then examined in terms of current densities and hydrogen recovery in MECs. The effect of applied voltage on catalytic activity of SS mesh and energy efficiencies was also important to evaluate for practical applications of the technology. Therefore the conditions with an applied voltages ranging from 0.6 to 1.2 V were examined with respect to hydrogen recovery to select an optimal applied voltage. A secondary objective was to examine new reactor configurations combining both low-cost carbon mesh anode and SS mesh cathodes with close electrode spacing in order to improve hydrogen production rate. The use of this architecture could be an effective way to further improve the useful configurations of electrodes in full-scale MECs.

Chapter 2

Literature Review

The new electrohydrogenesis process to produce hydrogen from biomass was first discovered independently by Liu et al.(17) and Rozendal et al. (17, 27, 28) in 2005 and the reactors are called microbial electrolysis cells (MECs) (Figure **2-1**) (20, 24, 29). The MEC has also been referred to as a biocatalyzed electrolysis cell (BEC) or a bioelectrochemically assisted microbial reactor (BEAMR) (17, 18, 28, 30, 31).

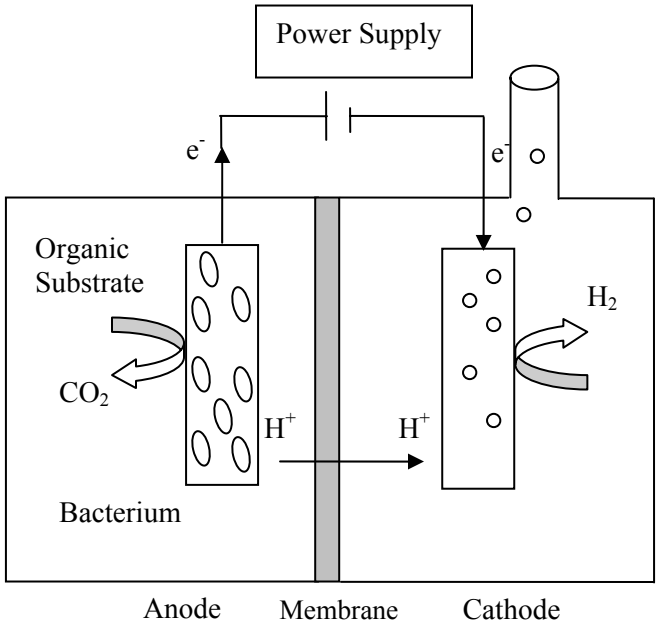

Figure 2-1: A General layout of a MEC in which in the anodic compartment the bacteria can bring about oxidative conversions while in the cathodic compartment reductive process produce hydrogen. (26)

The electrolysis-type process is based on modifying microbial fuel cells (MFCs). In an MFC, microorganisms oxidize organic matter and release carbon dioxide and protons into solution and transfer electrons to the anode electrode (32). Electrons travel through external circuit to the cathode, where they combine with oxygen to form water and current is generated.

The open circuit potential of the anode can approach the theoretical limit of ~ –0.3 V of the substrate (33, 34). Using acetate as a substrate, the anode reaction is:

$$\text{Anode: } C_2H_4O_2 + 2H_2O \rightarrow 2CO_2 + 8e^- + 8H^+ \quad (2\text{-}1)$$

The oxygen is prohibited at cathode in MECs while oxygen is needed as electron acceptor in MFCs. If hydrogen is produced at cathode, the cathode potential at pH=7 and 298°C is -0.414 V. The cathode reaction is:

$$\text{Cathode: } 8H^+ + 8e^- \rightarrow 4H_2 \quad (2\text{-}2)$$

The cell voltage under these conditions is negative:

$$E_{emf} = E_{cat} - E_{An} = (-0.414\ \text{V}) - (-0.3\ \text{V}) = -0.114\ \text{V} \quad (2\text{-}3)$$

The overall reaction is endothermic and requires a potential of at least –0.114 V in theory to produce hydrogen. In practice, applied voltage of ~ –0.2 V or more is needed between the anode and cathode due to overpotential at the electrodes (35). This voltage is much less than the voltage required for water electrolysis (–1.8 V– –2 V) (18). By using MEC device to capture protons and electrons from organic matter instead of water, hydrogen can be directly generated at a low voltage.

Hydrogen production by electrohydrogenesis is theoretically possible from any type of biodegradable organic matter that has been shown to produce electricity in a MFC, including carbohydrates (33-39), amino acids and proteins (40), and animal and human wastewaters (33, 41). Cheng et al. successfully examined the feasibility of using cellulose, glucose and five different volatile acids at an applied voltage of 0.6 V (29).

There are fewer studies of the microbial communities on the anodes of MEC than for MFCs. In MFCs, bacteria capable of electron transfer to an electrode, also named exoelectrogens, (18) include common genera such as *Geobacter*, *Shewanella*, *Pseudomonas* (42-46). *Pseudomonas* spp. and *Shewanella* spp. were found on the anode in MECs (47). Chae et al.

further demonstrated that *P.propionicus*-like species were dominant in the MECs and *Geobacter*-like species were still important members of the bacterial community. The augmentation of the circuit did not damage the bacterial viability in the MECs (48).

Most MEC reactors are two chamber systems separated by either cation or anion exchange membranes (CEM and AEM) (17, 18, 28, 48-53). The main purpose to use membrane is to avoid hydrogen diffusion losses from the cathode to microbes on the anode, where hydrogen could be consumed by hydrogenotrophic micro-organism (18, 23, 50). The membrane also prevents hydrogen gas from mixing with carbon dioxide in anode chamber to ensure high hydrogen concentrations in the cathode chamber. However, the presence of a CEM membrane can produce large pH gradients (50) across the membrane, which reduces pH in the anode chamber and elevates the cathode pH. This pH gradient caused a loss of 38% of the potential in the system in one study (50). The use of an AEM and high surface area anode graphite granules was found to substantially increase MEC performance at a hydrogen production rate of 1.1 m^3H_2/m^3d with overall efficiency of 82% using acetic acid as substrate at an applied voltage of 0.6 V (29).

A more simple and economical single-chamber MEC system that lacks a membrane was designed by Call et al. (20). A high hydrogen production rate of 3.12 m^3H_2/m^3d at an applied voltage of 0.8 V and a 78% overall energy efficiency was obtained which is comparable to that using a membrane. Hu et al. (54) showed that their membraneless MEC system could produce 0.53 m^3H_2/m^3d at 0.6 V. However, the lack of a membrane can affect gas purity by mixing hydrogen with carbon dioxide, and stimulating methane generation (18, 20, 23, 50). Methane generation is primarily a result of current generation and hydrogenotrophic methanogenesis (55). Several strategies to minimize methane have been suggested: exposing the reactor to air between feeding cycle (20); raising applied voltage and keeping cycle times short (55). Some chemicals

such as oxygen, 2-bromoethanesulfonate (BES) and acetylene are known to inhibit methanogenesis (56) and therefore were used for this purpose in MECs.

The same anode materials used in MFCs can also be used in MECs (32). Several carbon-based materials have been used as anodes, including carbon cloth (17), carbon paper (49), graphite felt (28, 50), granules (42, 57, 58) brushes (59), and carbon mesh (60). The performance of these materials depends on electrode spacing, solution conductivity and substrate (17, 61, 62). Brush anodes provide a high surface area for bacteria but they can also prohibit the whole electrode from being close to the cathode. It has been shown reducing electrode space from 4 cm to 2 cm using flat carbon cloth electrodes increased power from 18 to 60 W/m^3 (61). A low-cost flat carbon mesh as an alternative to expensive carbon cloth was examined by Wang et al. (60). The carbon mesh was pretreated at 450^oC for 30 min, resulting in a maximum power density of 46 W/m^3, which is comparable to or even exceeds performance of carbon cloth anodes. The use of carbon mesh anodes allows for close placement of the anodes next to the cathodes.

The performance of MEC has been greatly improved by using large surface area anodes, close electrode spacing, and different membrane materials. Nevertheless, designing efficient and economic cathodes remains a challenge. A precious metal such as platinum (Pt) on the cathode has been used in most studies to catalyze hydrogen evolution (17, 23, 27, 28, 31) because precious metal catalysts can reduce cathode overpotential by lowering the activation energy (63). The disadvantages of using platinum include its high cost and poisoning by chemicals such as sulfide (which is a common constituent of wastewater), resulting in reduced cathodic efficiency (23). Recently, a biocathode was developed as an alternative to a precious metal catalyst by Rozendal et al. (52), obtaining a current density of 1.2 A/m^2 at a cathode potential of –0.7 V. This result is substantially lower than the typical current densities range of 4-10 A/m^2 with a platinized electrode (17, 20, 54, 64). Several researchers have investigated new catalysts such as cobalt and iron cobalt tetramethylphenylporphyrin (CoTMPP & FeCoTMPP) (65), nickel oxide (66),

stainless steel (25, 66, 67), tungsten carbide (68). Among these studies, Call et al. (25) reported the highest hydrogen production rate of 1.7 m^3H_2/m^3d and overall energy efficiency of 78 % at an applied voltage of 0.6 V using low-cost high surface area stainless steel grade 304 brushes (650 m^2/m^3 of reactor volume, 0.5 cm electrode spacing).

Chapter 3

Material and Methods

3.1 Cathodes

Stainless steel alloys 304 (0.08% C, 2% Mn, 1%Si, 18-20%Cr, and 8-11%Ni (69)) woven (McMaster-Carr, IL) and expanded mesh (Dexmet Corporation, CT) were evaluated for their suitability as cathodes in MECs. Examples of both types of mesh are shown in Figure **3-1**. All the mesh were prepared for use in the MECs by cutting sheets of metal mesh into 3.8 cm diameter discs with an exposed projected surface area of 7 cm^2. Twelve SS 304 mesh of different sizes (Table **3-1**), one flat plate of SS 304, and laboratory-made carbon cloth (type B; E-TEK) with a platinum (Pt) catalyst (0.5 mg/cm^2) were tested in voltammetry tests. The three size ranges of SS meshes chosen for use in MECs were 44 × 44, 60 × 60, 165 × 165 and flat SS based on their characteristics: the largest pore size (>0.04 cm) for mesh #44, thick wire (~0.02 cm) and medium pore size for mesh #60 and the large measured active surface area (but smallest pore sizes) for mesh #165.

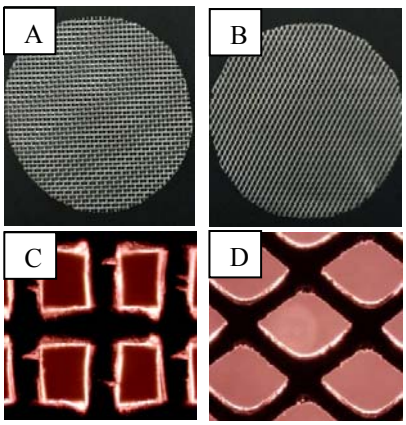

Figure 3-1: Types of SS 304 mesh used in studies: (A) and (C) are woven mesh, (B) and (D) are expanded mesh. (A) and (B) are 7 cm^2 round shape mesh, (C) and (D) are microscopic photos at 4 × magnification.

Table 3-1: SS meshes characteristics used in LSV and current magnitude distribution analysis.

Mesh number	Wire diameter / cm	Pore size / cm
30	0.030	0.030
42	0.014	0.046
44	0.014	0.044
50	0.014	0.037
60	0.011	0.031
60	0.019	0.023
80	0.009	0.022
80	0.014	0.018
90	0.014	0.015
120	0.010	0.011
165	0.0048	0.011
500	0.0025	0.0025

3.2 Electrochemical Analysis

Linear sweep voltammetry (LSV) was performed on a potentiostat (model PC4/750, Gamry Instruments, Warminster, Pennsylvania) over a range of 0 V to –1.5 V with a scan rate of –1 mV/s at 30ºC, in a 28 mL MFC reactor filled with 50 mM PBS (pH = 7.04). The three electrode LSV system contains a working electrode (cathode electrode), a counter electrode (platinum plate with a projected surface area of 2 cm^2), and a Ag/AgCl reference electrode (MF-2052, BASi, IN). The performance of flat SS and different types of SS 304 mesh (woven & expanded) was evaluated on the basis of voltage needed to initiate hydrogen production, V_e, and slope of the voltammogram V_h (65) shown in Figure **4-1**. The value of V_e demonstrates the ability of the catalyst to reduce overpotential while V_h indicates current production rate at applied voltage. The smaller the value of V_e and the larger the value V_h, the better the catalytic performance is. All the potentials shown in the results were versus standard hydrogen electrode (SHE) unless specialized.

Active surface areas of the different SS mesh were estimated by cyclic voltammetry (CV) using a ferrocyanide solution (70). A solution of 5 mM $K_4Fe(CN)_6$ containing 0.2 M

Na_2SO_4 deoxygenated with ultra high purity (UHP) nitrogen (99.998%) for 30 minutes was placed in the reactor described in the LSV method with a Pt/C cathode as the counter electrode. The cathode was wet-proofed (30%) carbon cloth (type B; E-TEK), with a surface area of 7 cm^2 and a platinum (Pt) catalyst (0.5 mg/cm^2). The reactor was assembled and filled with solution in an anaerobic glove box to avoid oxidation of ferrous ion. CV scans were conducted over the range of –0.3 to 1.2 V with a scan rate of 50 mV/s. The peak current, i_p (A) and effective area of the working electrode was obtained using Matsuda's equation:

$$i_p = 0.4464 \times 10^{-3} n^{3/2} \mathrm{F}^{3/2} A (\mathrm{R}T)^{-1/2} D_R^{1/2} C_R^* v^{1/2} \quad (3\text{-}1)$$

where n = 1 is the number of electrons transferred, F = 96487 C/mol is Faraday's constant, R = 8.314 J/mol ·K is the gas constant, T = 303 K is the temperature, C_R^* =0.005 mol/L is the initial ferrocyanide concentration, and v = 0.05 V/s is the scan rate. The diffusion coefficient of $K_4Fe(CN)_6$ was calculated as D_R =2.66 × 10^{-6} cm^2/s from the value of i_p using equation **3-1** with a SS flat sheet as the working electrode (surface area = 7 cm^2), which is comparable with that previously reported (～6.5 × 10^{-6} cm^2/s; 0.1 $mol \cdot L^{-1}$, 25 °C) (70). The stainless steel was cleaned before tests using 0.5 M H_2SO_4. Based on the above given values, the equation for the electrochemical active area (cm^2) can be simplified to $A = 2.058 \times 10^3 \times i_p$.

3.3 MEC Reactor Construction and Operation.

3.3.1 Single-cell Cubic Reactor

The MEC used for mesh comparison in this study was a single-cell cubic reactor as described by Call et al. (20). This reactor is formed from a solid block of Lexan and is cube-shaped, containing a cylindrical chamber (4 cm long, 3 cm diameter, empty bed volume of 28 mL) (Figure **3-2**). The anode was an ammonia-treated graphite brush (25 mm diameter × 25 mm

length; 0.22 m^2 surface area; fiber type: PANEX 33 160K, ZOLTEK), with a specific surface area of 18,200 m^2/m^3 and porosity of 95% (20).

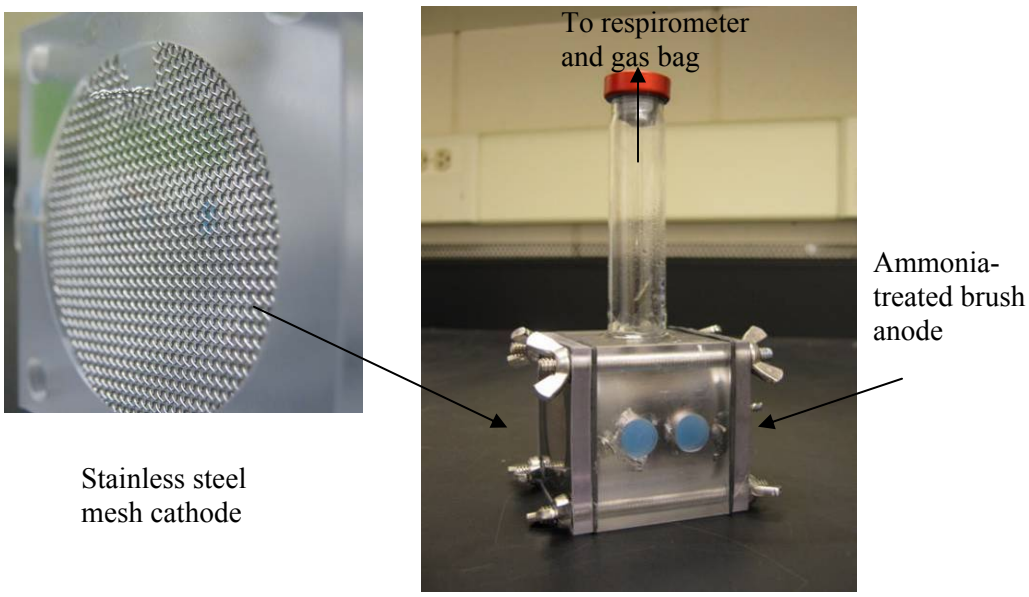

Figure 3-2: MEC reactor with an 8 cm gas collection tube, a stainless steel mesh cathode (left, the cathode was bent to have an opening at the top) and an ammonia-treated brush anode (right)

The brush anodes were first inoculated in single-chamber cubic MFCs with Pt/C flatcathodes (71). The MFCs were fed a pre-acclimated suspension of bacteria solution (50% v/v) from an acetate-fed (1 g/L) MFC bottle-type reactor running for more than 1 year, and a buffer nutrient medium consisted of a 50 mM PBS phosphate buffer (4.58 g/L Na_2HPO_4, and 2.45 g/L $NaH_2PO_4 \cdot H_2O$, pH=7.04), 0.31 g/L NH_4Cl, 0.13 g/L KCl, trace vitamins and minerals (71)) containing 1 g/L sodium acetate as substrate. After a reactor reached maximum voltage for at least 3 cycles, the anode was considered acclimated and was transferred to an MEC.

MECs (duplicates) were operated in fed-batch mode. To avoid gas accumulation between mesh cathode and end plate, a portion of the top of the mesh was cut off and bent into the solution to assure no surface area loss as shown in Figure **3-2**. All gas produced at the cathode was collected into an anaerobic gas collection tube (8 cm high, 1.6 cm in diameter and 15 mL in volume) glued to the top of the cubic reactor. The gas-collection tube was sealed by a butyl

rubber stopper and an aluminum crimp cap. Gas production was measured using a respirometer (AER-200; Challenge Environmental) (20, 29). The gas produced was then collected in a gas bag (0.5 L capacity; Cali-5-Bond, Calibrated Instruments Inc.). After each cycle, the anode was exposed to air for 20 to 30 minutes to limit the growth of methanogens (20). The MEC reactors and gas bags were sparged with UHP N_2 for 15 minutes to remove O_2 from the reactor (20). The gas bags were then vacuum sealed. All batch experiments were conducted at 30ºC and the pressure was assumed equal to 1 atm. 10 mM 2-bromoethanesulfonate (BES), an analogue of coenzyme M (72) was used to inhibit methanogens at applied voltage of 0.6 V.

A power source (model 3645 A; Circuit Specialists, Inc.) was used to apply voltage ranging from 0.6 to 1.2 V to the MECs. A multimeter (model 2700; Keithley Instruments, Inc.) (49) was used to record the voltage across the resistor. Current was calculated using Ohm's law ($I = V/R$, $R = 10\ \Omega$). The end of the batch was determined by the end of the gas production and the sharp decrease in current production. New cathodes were used for each applied voltage. Total chemical oxygen demand (COD) was measured at the beginning and end of each batch (TNT plus COD Reagent; HACH Company).

3.3.2 Bottle Reactor

To improve the MEC performance, three kinds of sandwich-type electrodes were used to reduce electrode spacing (Figure **3-3**). The anode electrodes were heat treated carbon mesh (Gaojieshi Graphite Products Co. Ltd., Fujian, China) (60). The cathodes were SS mesh #60. The difference among three electrode arrangements was the separators placed between two electrodes. The first type of the separators was glass fiber mats (GF) with thicknesses of 1 mm (type DC1.0, Jiafu Co., China) (73). The second type was round-hole perforated plastic separator (SEP) with a thickness of 1.5 mm and porosity of 40% (McMaster-Carr, IL). The third type construction (EMP)

used two pieces of a small plastic separator described above to support the top and bottom of electrodes, leaving an empty space between the electrodes of 1.5 mm. Each electrode was 8 cm^2 and the separator was 10 cm^2. The reactors were bottles (135-mL capacity, filled to 110 mL) with the electrodes hanging in the middle of the reactors. There was no separate inoculation for mesh anodes. The bottle MECs were first fed a preacclimated suspension described in cubic reactors and 1 g/L sodium acetate as substrate. After hydrogen was produced, the reactors operated as in normal MECs.

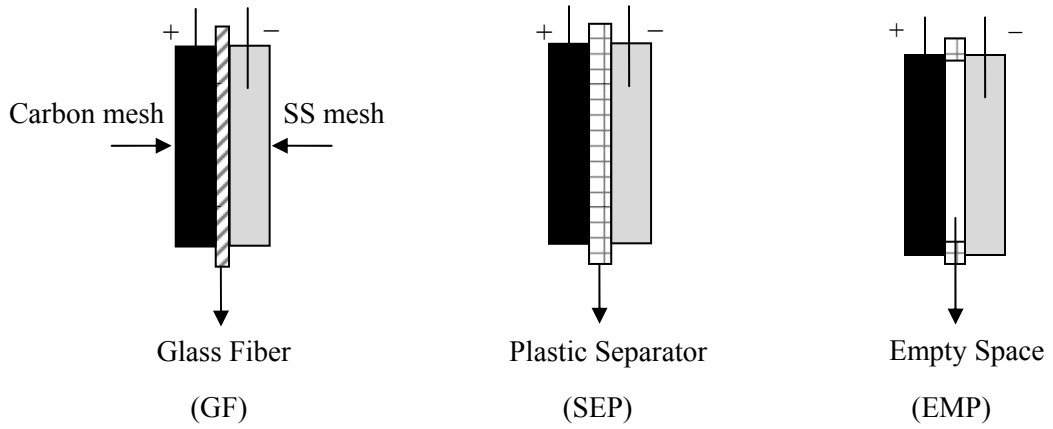

Figure 3-3: Schematic of sandwich-type electrodes in different configurations.

3.4 Gas Analysis

The composition of the MEC headspace and gas bags were analyzed using gas chromatography (49). Samples (200 μL) were taken with a gas-tight syringe (250 μL, Hamilton Samplelock Syringe) in duplicate from the MEC head space, and in triplicate for the gas bags. N_2, H_2, and CH_4 were analyzed with one gas chromatograph (GC) (argon carrier gas; model 8610B; SRI Instruments), and CO_2 with a separate GC (helium carrier gas; model 310, SRI Instruments). Standard curves were prepared with pure N_2, H_2, CH_4, and CO_2 samples. N_2 was a dilution gas

and therefore it was removed in the calculations to find the concentrations of H_2, CH_4, and CO_2 produced by the system (23).

3.5 Calculations

The performance of the mesh cathodes was evaluated using volumetric current density, hydrogen recovery, hydrogen production rate, and the energy recovery (electrical and overall energy) as described in Call et al. (20) and Logan (18, 23), and summarized below.

3.5.1 Hydrogen Yield and Production Rate

The theoretical maximum hydrogen yield of moles (n_{th}) based on COD consumption is:

$$n_{th} = \frac{2 V_L \, \Delta\mathrm{COD}}{M_{O_2}} \tag{3-2}$$

where 2 is the ratio of electron equivalent per mole of oxygen to the electron equivalent per mole of hydrogen (18). V_L= 30 mL is the liquid volume in the reactor, ΔCOD (g COD/L) is the change of COD in substrate concentration, and M_{O2} = 32 g/mol is the molecular weight of the oxygen. The theoretical number of hydrogen moles that can be recovered based on the current (n_{CE}) is:

$$n_{CE} = \frac{\int_{t=0}^{t} I \, \mathrm{d}t}{2F} \tag{3-3}$$

where $I = V/R_{ex}$ is the current (A) calculated from the voltage measured across the 10 Ω resistor using Ohm's law, dt is the time interval (20 minutes), 2 is the number of moles of electrons per mole of hydrogen produced, and F = 96,485 C/mole e^- is Faraday's constant.

The Coulombic hydrogen recovery (Coulombic Efficiency) (r_{CE}) is calculated as the number of electrons recovered in the circuit compared to the maximum theoretical hydrogen available from the substrate consumed:

$$r_{CE} = \frac{n_{CE}}{n_{th}} = C_E \tag{3-4}$$

The cathodic hydrogen recovery (r_{cat}) is the fraction of electrons that are recovered as hydrogen from the total number of electrons that reach the cathode:

$$r_{cat} = \frac{n_{H_2}}{n_{CE}} \tag{3-5}$$

where n_{H2} is the number of moles of hydrogen produced by the system during a batch cycle.

The overall hydrogen recovery (r_{H2}) was calculated as:

$$r_{H_2} = \frac{n_{H_2}}{n_{th}} = r_{Cat}\, C_E \tag{3-6}$$

The maximum volumetric hydrogen production rate Q_{H2} in m^3/m^3-d is calculated as:

$$Q_{H_2} = 3.68 \times 10^{-5}\, I_V\ T\, r_{cat} \tag{3-7}$$

where 3.68×10^{-5} is a constant that includes Faraday's constant, 1atm pressure and unit conversions, I_V (A/m^3) is the volumetric current density averaged over 4 hour period of maximum current production for a batch cycle normalized by the liquid volume of the reactor, and T is the temperature in Kelvin .

3.5.2 Energy Recovery

The energy efficiency relative to electrical input (η_w) can be calculated from the ratio of energy content of hydrogen produced to the electrical energy input as:

$$\eta_w = \frac{W_{H_2}}{W_E} \tag{3-8}$$

The energy content of hydrogen calculated from its heat of combustion ΔH_{H2} (kJ/mol), as:

$$W_{H_2} = n_{H_2}\, \Delta H_{H_2} \tag{3-9}$$

where $\Delta H_{H2} = 285.83$ kJ/mol is the heat of combustion of hydrogen gas.

The electrical energy added to the system by the power source, accounting for losses in the resistor (W_E) is:

$$W_E = \sum_{t=0}^{t} (IE_{ap}\Delta t - I^2 R_{ex}\Delta t) \tag{3-10}$$

where I is the current calculated as before, E_{ap} is the voltage applied to the reactor, R_{ex} is the external 10 Ω resistor, and Δt is the time interval between two data points (20 minutes). The electrical energy efficiency η_w can be over 100% because it does not take into account the energy input coming from the substrate. The energy efficiency relative to the substrate (η_s) is:

$$\eta_S = \frac{W_{H_2}}{W_S} \tag{3-11}$$

The energy content of the substrate is:

$$W_S = n_S\, \Delta H_S \tag{3-12}$$

Where $\Delta H_S = 870.28$ kJ/mol is the heat of combustion of the substrate and n_s is the number of moles of substrate consumed during a batch cycle based on COD removal:

$$n_S = \frac{\Delta \text{COD}\ V_L}{M_S \times 0.78\,\text{g COD}\cdot\text{g}^{-1}} \tag{3-13}$$

where M_s = 82 g mol^{-1} is the sodium acetate molecular weight and 0.78 gCOD g^{-1} is the conversion factor of sodium acetate.

The overall energy efficiency (η_{w+s}) which takes into account both the electrical and the substrate energy input is calculated as follows:

$$\eta_{w+s} = \frac{W_{H_2}}{W_E + W_s} \tag{3-14}$$

Chapter 4

Results

4.1 Evaluation of Mesh Type

The most effective catalyst, our laboratory-made Pt/CC cathode, required a potential of –0.38 V for current production. The value of V_e was similar for different type mesh at –0.67 ± 0.01 V. Based on the mesh cathode overpotential obtained from LSVs, a minimum of 0.42 V would be required for hydrogen production in an MEC for the SS 304 mesh catalyst, assuming an anode potential of –0.25 V (18).

Woven mesh #44 was more effective in increasing current than expanded mesh, as shown by the values of V_h in Table **4-1**. Woven mesh #44 and expanded mesh possess approximately the same wire thickness (~0.015 cm) and pore opening area (~0.0025 cm^2). The calculated surface area was very close for woven mesh (9.25 cm^2/ 7 cm^2) and expanded mesh (8.88 cm^2/ 7 cm^2) based on mesh characteristics shown in Table **4-1**. The larger current per applied voltage of woven mesh #44 could result from difference between active surface area and calculated values due to the woven construction. Current production was substantially lower for the expanded mesh than woven mesh at larger currents. The mesh pattern could influence bubble entrapment. As a result of these tests, SS 304 woven mesh was considered to be a more effective catalyst for hydrogen evolution in MECs and was used in further studies.

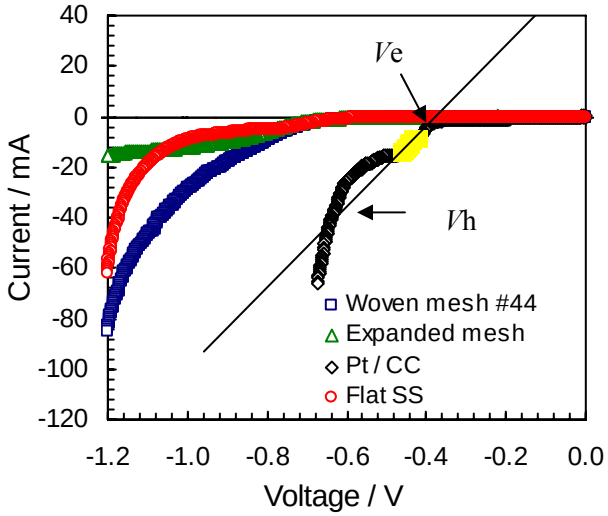

Figure 4-1: LSV curves for the SS 304 woven mesh #44, expanded mesh, flat SS and platinum carbon-cloth.

Table 4-1: Evaluation of different catalyst in terms of minimum required voltage (V_e) and slope of the applied voltage (V_h).

Material	Wire size / cm	Pore opening area / cm^2	V_e / V	V_h / mA V^{-1}
Woven mesh 44	0.014	0.00023	-0.68	81.48
Expanded mesh	0.015	0.00025	-0.67	47.64
Flat SS	-	-	-0.66	32.54
Pt / CC	-	-	-0.38	159.72

4.2 Mesh Characteristics

The surface areas of 12 different size meshes (Table **3-1**) were both calculated and measured from CVs based on normalizing values to the 7 cm^2 of projected cathode area. The range of electrochemical active areas measured in CV tests compared reasonably well (12.23 to 23.26 cm^2) to the calculated values (9.71 to 20.15 cm^2). However, the difference between calculated and measured values varied for individual mesh. For example, mesh #30 with a relatively thick wire of 0.03 cm had an 87% larger active area than the calculated area. The largest active area mesh was #120 with 23.26 cm^2, which is three times larger than flat SS of the same projected surface area (Table **4-2**). The difference between the largest and smallest active

surface area was 11.03 cm^2. The larger values of measured active surface area than that calculated are possible due to the underestimation of junction areas or surface roughness (see a calculation example in **Appendix A**).

Table 4-2: Areas based on mesh properties and electrochemically active areas measured by CV.

Mesh number	i_p / mA	Calculated Area / cm^2	Measured Area / cm^2	Difference / %	Specific Surface Area / $m^2 \cdot m^{-3}$ reactor volume
flat	3.40	7	7	-	23.33
30	9.50	10.45	19.56	87	65.20
42	5.94	9.71	12.23	26	40.77
44	6.00	10.26	12.35	20	41.18
50	6.62	11.54	13.63	18	45.43
60	7.84	11.32	16.14	42	53.80
60	9.61	17.77	19.79	11	65.95
80	7.30	12.24	15.03	23	50.10
80	8.31	17.52	17.11	-2	57.03
90	8.24	20.15	16.96	-16	56.55
120	11.30	18.71	23.26	24	77.55
165	8.96	12.89	18.45	43	61.49
500	7.55	19.30	15.54	-19	51.81

4.3 Hydrogen Evolution Rate Using Different Size Mesh

LSV scans were performed on 12 mesh cathodes (characteristics shown in Table **3-1**). The impact of mesh characteristic including mesh number, wire diameter, pore size and surface area was first evaluated based on their correlation with current distribution using LSV results (Table **4-3)**. The larger the positive coefficient, the more important this factor was indicated to be for current generation. A negative coefficient indicates an inverse relationship between impact factor and current. While the importance of the different factors varied with the current range, the most significant impact factors were wire diameter and pore size. In the low current range, the wire diameter was dominant, having a coefficient of 0.68~0.70. The measured active surface area was closely related to the wire thickness, as shown by a coefficient of 0.90. Therefore, the larger active

surface area was the most critical factor at low current for improving current generation. In the medium current range, the importance of pore size was indicated to be substantially more important, increasing from a factor of 0.3 to 0.8–0.9. In the high current range, both wire diameter and pore size equally affected current generation. The small and negative coefficient between calculated area and current generation confirmed that the true active area of meshes was not consistent with the value calculated from mesh characteristics (coefficient of 0.14 between these two areas).

Table 4-3: Correlation factors between current and SS mesh number, wire diameter, pore size, calculated surface area and measured electrochemical active area.

		mesh number	**wire diameter**	**pore size**	**Calculated Area**	**Measured Area**
mesh number		1.00				
wire diameter		-0.63	1.00			
pore size		-0.68	0.48	1.00		
Calculated Area		0.49	-0.29	-0.80	1.00	
Measured Area		-0.46	0.90	0.10	0.14	1.00
Current range / mA	Cathode Potential / (V vs. SHE)					
1~10	-0.6	-0.70	0.70	0.29	0.07	0.76
	-0.7	-0.60	0.68	0.28	0.03	0.74
	-0.8	-0.68	0.68	0.36	-0.06	0.69
10~40	-0.9	-0.82	0.63	0.82	-0.48	0.42
	-1.0	-0.72	0.62	0.91	-0.57	0.33
	-1.1	-0.62	0.59	0.80	-0.43	0.36
>40	-1.2	-0.41	0.47	0.39	0.04	0.47

At low current, small hydrogen bubbles began evolving on the mesh wire. The bubble coverage was small because of the low current generation (Figure **4-2.A).** As the current increased, the bubbles expanded with time until the size of hydrogen bubbles equaled the mesh pore size. The bubble coverage appeared the largest at this time (Figure **4-2.B)**. With a further current increase, some of the bubbles fused and formed larger break-off bubbles on the mesh surface. Most bubbles departed so that new bubbles could evolve on the vacant places (Figure **4-3.C)**.

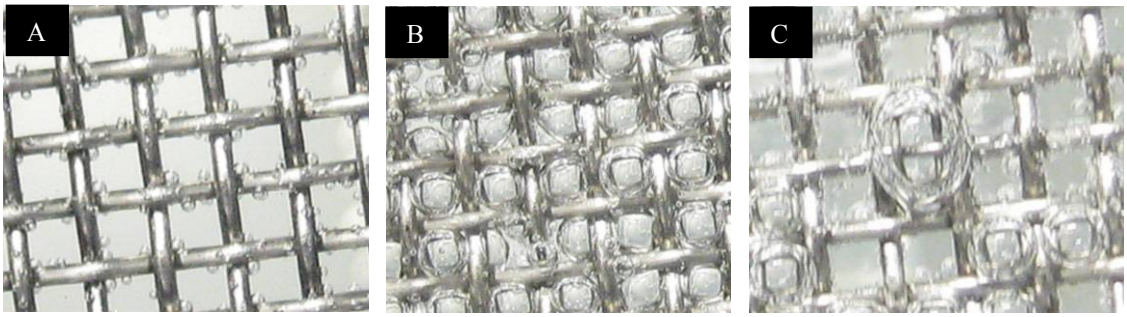

Figure 4-2: Hydrogen bubble visualization on SS mesh at 5 mA (A), 40 mA (B), 80 mA (C)

To further quantitatively describe the optimal wire diameter and pore size, the currents for the 12 mesh at each applied voltage in LSV tests was plotted in 3-dimensional coordinates with the *z* axis as current , the *x* axis as the wire thickness and *y* axis as opening size (pore size). Griddata, which is an interpolation function in Matlab, was used to define the type of surface fit to the data (74). The red color in the map indicates larger currents while blue is the color of the lowest currents. Three current ranges (low current: 1~10 mA; medium current: 10~40 mA; large current: >40 mA) were selected on the basis of factors that appeared to produced similar results (Table **4-3)**.

In the low current range, the largest current falls on the region where wire thickness is between 0.02 to 0.03 cm and pore size is between 0.02 and 0.03 cm (Figure **4-3.A**). The largest current generation was observed on Mesh #60, with a wire diameter of 0.019 cm and a pore size of 0.023 cm. In the medium current range, the best current production region moved towards pore sizes larger than 0.04 cm, while the optimal wire thickness remained 0.02 to 0.03 cm (Figure **4-3.B**). Mesh #42 and #44 with the largest pore sizes, performed the best. The preferred pore size shifts back to the smaller value (less than 0.03 cm) in the large current range (Figure **4-3.C**). Mesh #60 again was the best mesh of current generation in this large current range.

(A)

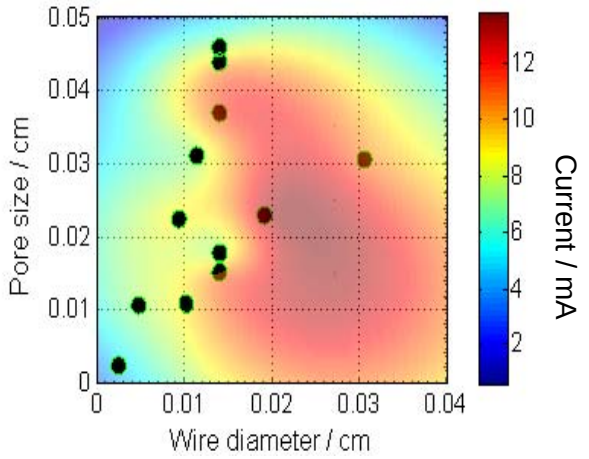

(B)

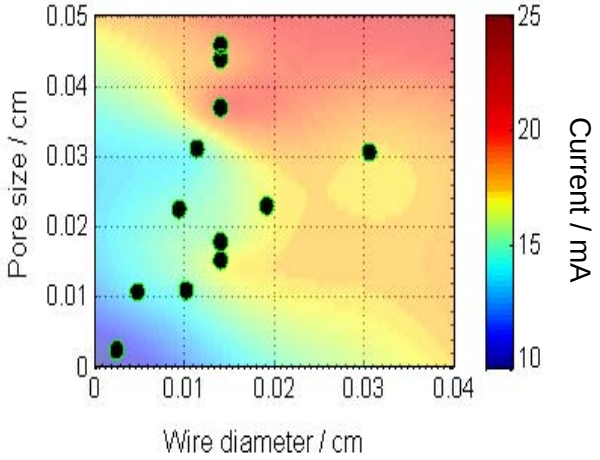

(C)

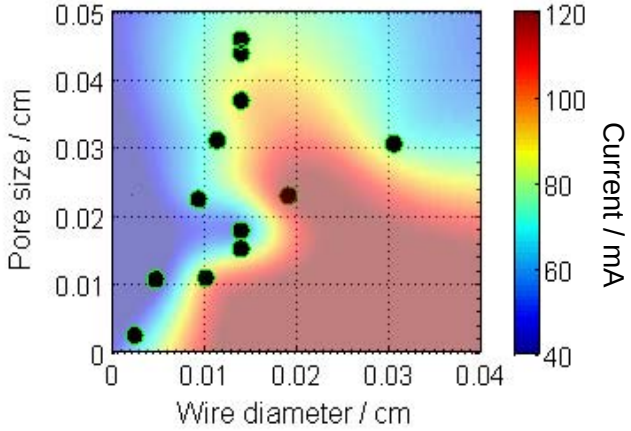

Figure 4-3: Current magnitude distribution versus mesh wire diameter and pore size at low current (A), medium current (B) and large current (C)

4.4 Current Densities and Maximum Hydrogen Production Rates in MECs.

Flat SS as a control and mesh #60 were used in MEC tests to preliminarily determine the SS mesh behavior at different applied voltages. The currents obtained using flat SS increased with the applied voltage from 1.6 mA (0.6 V) to 7.8 mA (1.2 V), and with mesh #60 from 2.5 mA (0.6 V) to 7.4 mA (1.1 V) (Figure **4-4**). These values are within the small current range defined above. The current–anode potential curve showed an S-shaped response (Figure **4-5**), which is the typical characteristic of the electrical potential term effect on current (i.e., the Nernst-Monod term) (75). As the applied voltage increased from 1.1 V to 1.2 V, the cathode had a relatively constant potential, while the anode potential sharply decreased from –0.14 V to –0.076 V for flat SS and –0.13 V to –0.05 V for mesh #60. The maximum current measured was 7.6 ± 0.3 mA and the current was saturated at an anode potential over –0.1 V.

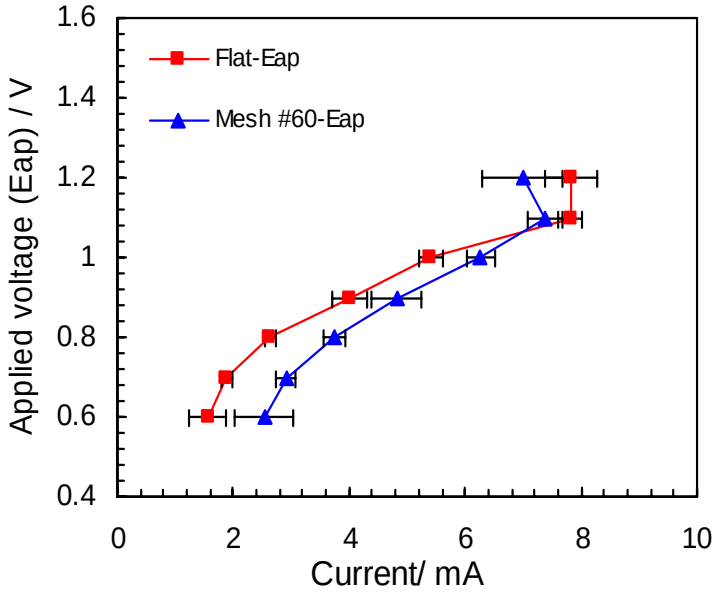

Figure 4-4: Current as a function of applied potential in cubic single cell MEC for flat SS and SS mesh #60 cathodes.

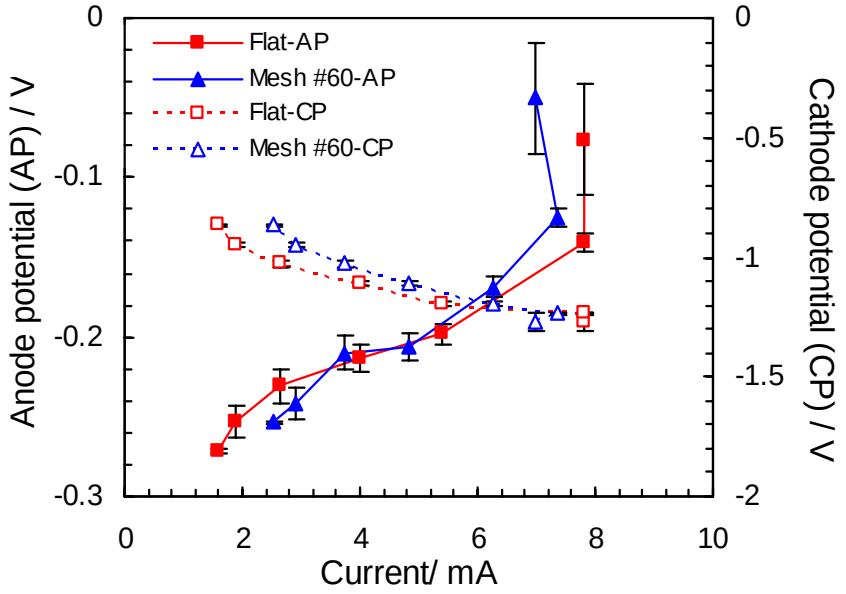

Figure 4-5: Current as a function of cathode and anode potential in cubic single cell MEC for flat SS and SS mesh #60 cathodes.

To examine the optimum mesh characteristics in MECs at a relatively high current (E_{ap} = 1.2 V), medium current (E_{ap} = 0.9 V) and low current (E_{ap} = 0.6 V), mesh #44, #60 and #165 were compared for current densities and maximum hydrogen production rates. The volumetric current density of mesh #60 was highest among the three meshes at each applied voltage. The current density of mesh #44 was slightly lower than #60 at each applied voltage (Figure **4-6**). The difference between mesh #60 and #44 was about 5 A m^{-3} at applied voltages of 1.2 V and 0.9 V, and 12 A m^{-3} at 0.6 V. Mesh #165 produced the lowest current density and a difference was observed of ~20–40 A m^{-3} from the two mesh (Table **4-4**). Mesh #60 always produced the largest maximum hydrogen production rates, with 3.3 ± 0.4 m^3H_2/m^3-d at 1.2 V, 2.1 ± 0.3 m^3H_2/m^3-d at 0.9 V, and 0.8 ± 0.1 m^3H_2/m^3-d at 0.6 V (Table **4-4**).

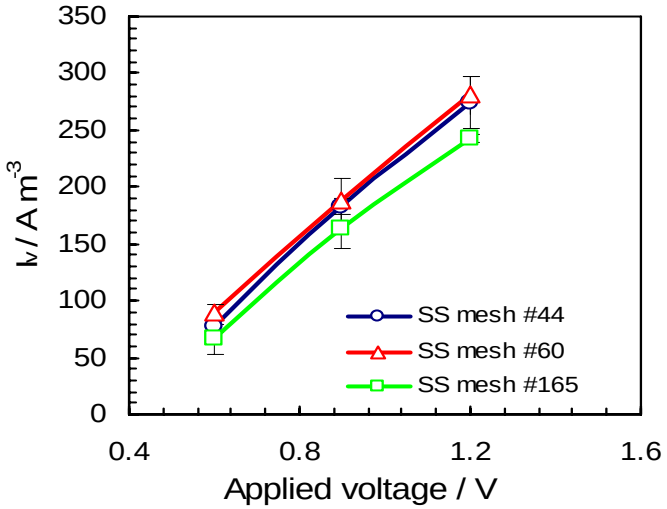

Figure 4-6: Volumetric current densities, *I*v, comparison as a function of applied voltage for SS mesh #44, #60 and #165 cathodes.

Table 4-4: Volumetric current density I_v and maximum hydrogen production rate Q of different meshes at different applied voltage.

Mesh Number / **Applied Voltage / V**	**44**	**60**	**165**
	Current density I_v / A m^{-3}		
1.2	275 ± 23	281 ± 17	243 ± 4
0.9	183 ± 7	188 ± 19	164 ± 17
0.6	78 ± 7	90 ± 7	67 ± 13
	Maximum hydrogen production rate Q / m^{3}H$_2$/m^3-d		
1.2	2.66 ± 0.05	3.30 ± 0.38	2.53 ± 0.09
0.9	1.73 ± 0.03	2.10 ± 0.28	1.46 ± 0.03
0.6	0.64 ± 0.04	0.83 ± 0.13	0.45 ± 0.02

4.5 Cathode Potential

SS mesh #60 required the lowest applied voltage to start producing hydrogen (Figure **4-7,** Table **4-5**) and it exhibited the lowest cathode potential at different applied voltage in MECs (Figure **4-8**). The cathode potential of mesh #165 was lower than mesh #60, especially at higher applied voltage. A cathode potential 30 mV larger than for mesh #60 was observed using mesh #165 at 1.2 V. The flat SS with the least surface area produced the highest cathode potential in MECs (Figure **4-8,** Table **4-5**).

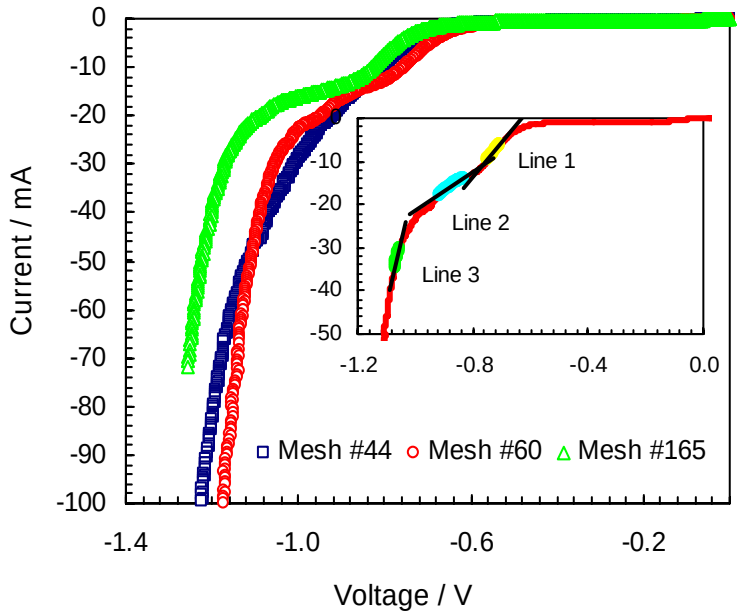

Figure 4-7: LSV curves for different mesh cathodes tested in MECs (cathode voltage is versus SHE). Three lines in each linear current range were to show the hydrogen bubble effect which will be analyzed in discussion part 3.5.1.

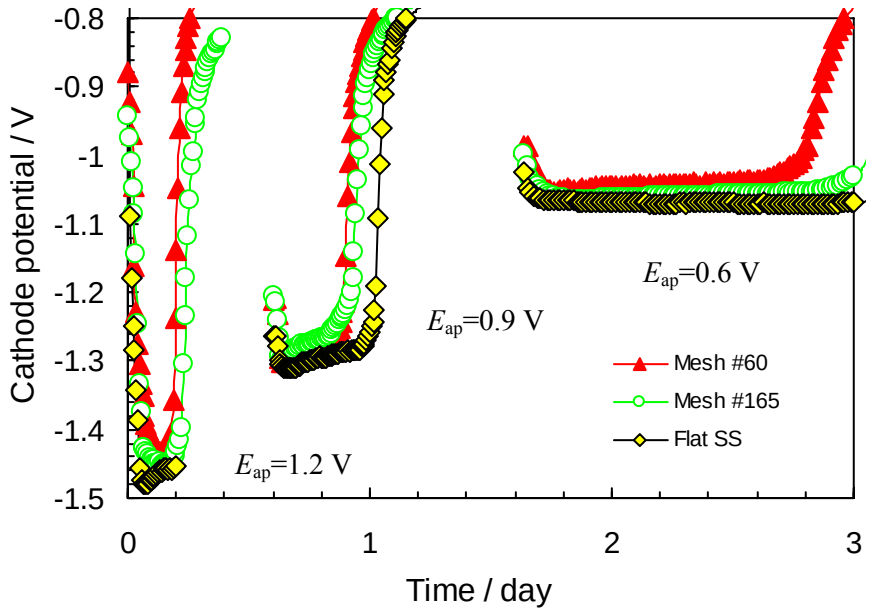

Figure 4-8: Cathode potential (versus Ag/AgCl) versus time using flat SS and SS mesh cathodes at E_{ap} = 1.2 V, 0.9 V and 0.6 V.

Table 4-5: Comparison of meshes in terms of minimum required voltage (V_e) by LSV and cathode potential in MECs at different applied voltage.

Mesh number	**Cathode potential / V (vs. SHE)**			
	LSV: V_e / V	MEC		
		E_{ap} = 0.6 V	0.9 V	1.2 V
44	-0.68	-	-	-
60	-0.63	-0.85	-1.10	-1.22
165	-0.72	-0.86	-1.09	-1.25
Flat SS	-0.66	-0.87	-1.10	-1.27

4.6 Hydrogen Recovery

The coulombic efficiencies reached peak values at 0.8 V for both the flat SS and mesh #60 at 123 ± 4 % and 101± 1%. The same trend in hydrogen recovery on the cathode was observed for flat SS and mesh #60. The hydrogen recovery at applied voltages of 1–1.2 V were similar and close to 100%. The hydrogen recoveries decreased with the applied voltage decrease, with the r_{cat}% of flat SS decreasing to 15 ± 2% and r_{cat}% of mesh #60 to 78 ± 3%. The overall hydrogen efficiencies were determined by both coulombic efficiency and cathodic hydrogen recovery, and reached the highest values at 1.1 V (Figure **4-9**).

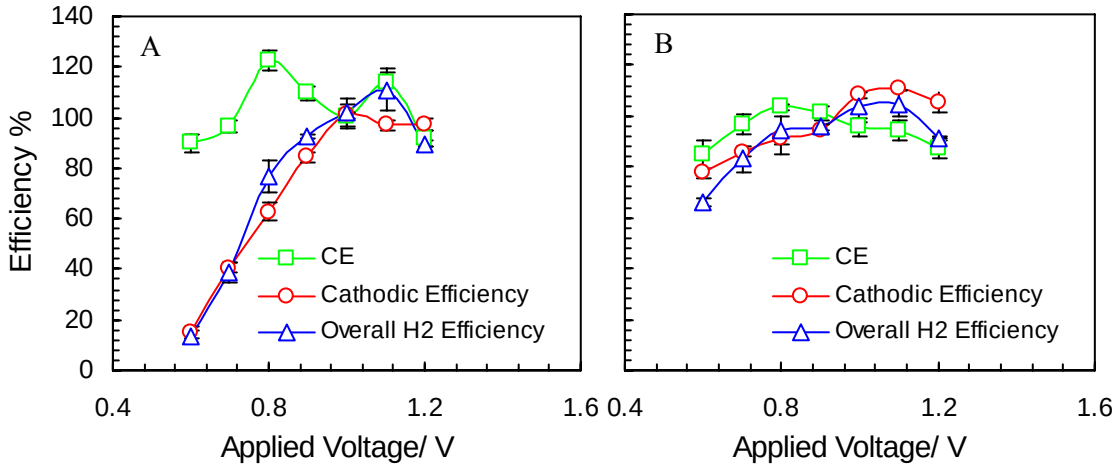

Figure 4-9: Coulombic efficiency, cathodic hydrogen recovery efficiecy and overall hydrogen efficiency as a function of applied voltage for flat SS (A) and SS mesh #60 (B).

The percentage of methane of flat SS increased from 0% to 47.4 ± 2.8 % and mesh #60 from 0% to 4.6 ± 1.1 % as the applied voltages decreased from 1.2 V to 0.6 V. Methane first appeared at 0.8 V for the flat SS, and 0.7 V for SS mesh #60. Methane accumulation was due to the long operation cycles needed at the lower applied voltages (32). The hydrogen production decreased down to 4.2 ± 0.6 ml for flat SS and 22.6 ± 0.1 ml for SS #60 (Figure **4-10**).

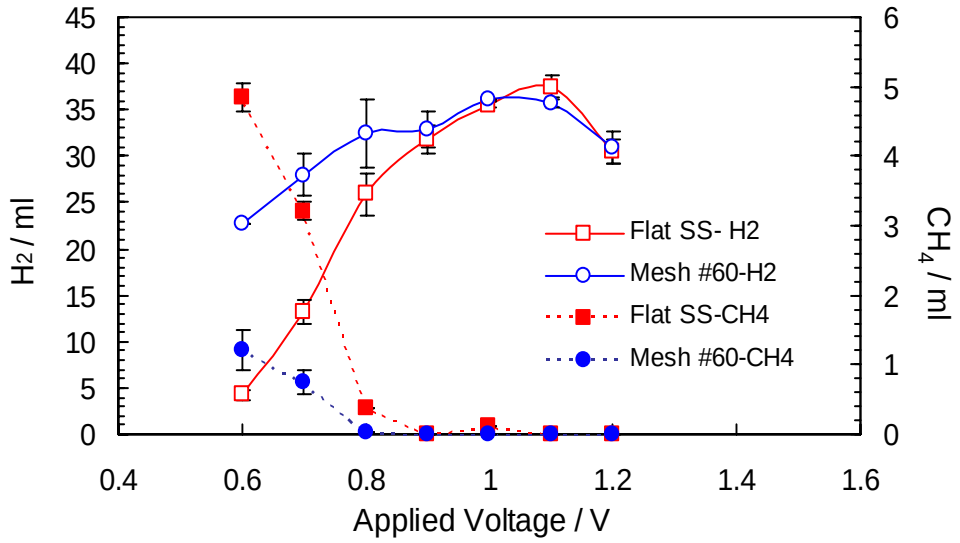

Figure 4-10: Hydrogen (solid line), methane (dash line) volume at each applied voltage for flat SS (square symbol) and SS mesh #60 (round shape symbol).

Three mesh comparisons showed that the highest cathodic hydrogen recovery was achieved using mesh #60 at 105 ± 8 % at 1.2 V, 99 ± 7 % at 0.9 V and 83 ± 7 % at 0.6 V (Table **4-6**). No methane was detected due to the short term operation of the tests. However, the difference of r_{cat} among three mesh was not significant. The r_{cat} decrease with a voltage decrease was also observed. The COD removal of all three meshes at different applied voltages was fairly constant at about 92 ± 1%.

Table 4-6: Summary of MEC hydrogen recovery and COD removal for different mesh cathodes.

Applied Voltage	Mesh	r_{CE} / %	r_{cat} / %	R_{H2} / %	H_2 / ml	COD/ %
1.2	44	90 ± 6	87 ± 5	78 ± 0	27 ± 1	91 ± 0
	60	91 ± 6	105 ± 8	96 ± 6	31 ± 2	92 ± 3
	165	87 ± 3	94 ± 5	81 ± 7	28 ± 1	91 ± 0
0.9	44	101 ± 14	85 ± 5	85 ± 7	30 ± 2	93 ± 1
	60	99 ± 3	99 ± 7	98 ± 4	35 ± 0	94 ± 2
	165	106 ± 2	81 ± 7	85 ± 9	30 ± 1	91 ± 3
0.6	44	102 ± 22	74 ± 11	74 ± 5	26 ± 4	92 ± 4
	60	96 ± 15	83 ± 7	80 ± 19	27 ± 4	93 ± 2
	165	116 ± 18	61 ± 9	71 ± 10	25 ± 0	92 ± 2

4.7 Comparison of Hydrogen Recovery with and without Methane Production

BES was added into MECs in the first cycle at low applied voltages of 0.6 V. No methane was then detected in the subsequent three cycles. The average hydrogen production with a flat SS cathode and a new anode (no methane production) was 17.0 ± 0.7 ml. The volumetric conversion from CH_4 to H_2 is 1:4. Based on this conversion, the predicted amount of hydrogen recovered from methane would be 23.7 ± 0.6 ml using an old anode. The average hydrogen production using mesh #60 with a new anode and BES was 29.3 ± 1.2 ml, which is 2 ml larger than the predicted volume of 27.5 ± 0.1 ml with a used anode and no BES (Figure **4-11**). The cathodic hydrogen recovery value calculated on MECs without methane production at 0.6 V were 57 ± 7 % for flat SS and 94 ± 8 % for mesh #60, marked by closed symbol in Figure **4-12**. The value was larger than that of MECs when methane was produced at 0.6 V but still smaller than the hydrogen recovery at higher applied voltage (≥ 0.9 V).

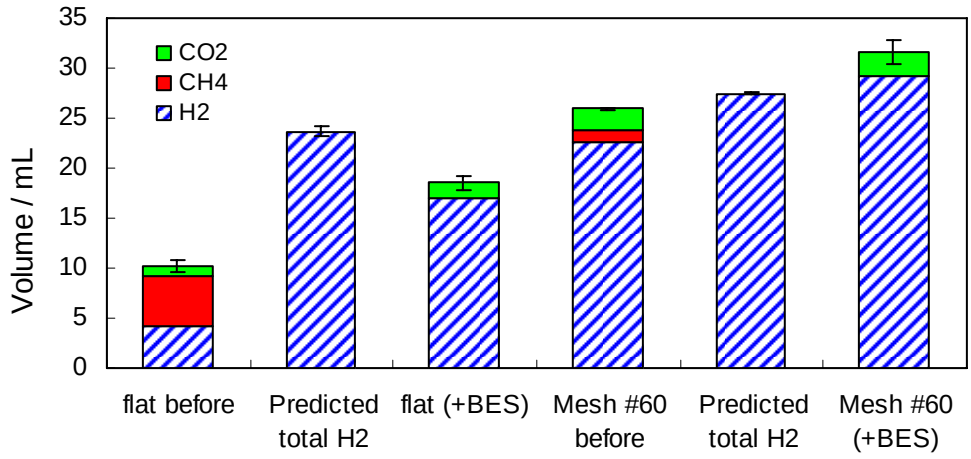

Figure 4-11: Gas composition for MECs with flat SS and mesh # 60 cathodes using old anode with methane existence and new anode adding BES at E_{ap} = 0.6 V. Error bar of MECs with used anode are based on duplicate measurements, error bar of MECs with new anode are based on three consecutive batch cycles.)

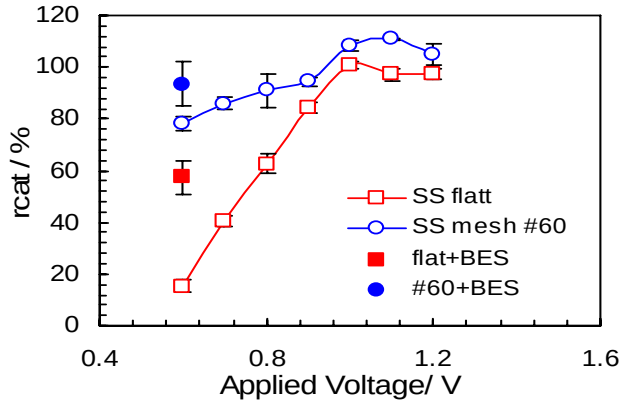

Figure 4-12: Cathodic hydrogen recovery as a function of applied voltage for flat SS and SS mesh #60 cathodes with used anode (open symbols) and new anodes after adding BES (filled symbols).

4.8 Electrical Energy Efficiency and Overall Energy Recoveries

The electrical energy efficiency η_w % only takes into account the electrical energy input excluding the substrate energy input and thus its value can be above 100%. Higher electrical energy efficiencies were obtained at the lower applied voltages. The energy recovery using mesh #60 at an applied voltage of 0.6 V reached the highest value of 232 ± 9 % (Table **4-7**). The overall energy recovery based on both substrate and electricity input is smaller than 100%. Mesh #60 produced the highest overall energy efficiency at 0.9 V with 74 ± 4%. A similar overall efficiency of 72 ± 11% was reached at 0.6 V.

Table 4-7: Summary of MEC energy efficiencies for different mesh cathodes.

Applied Voltage / V	Mesh	η_w / %	η_{w+s} / %
1.2	44	112 ± 4	54 ± 1
	60	138 ± 2	66 ± 3
	165	122 ± 6	57 ± 4
0.9	44	136 ± 8	61 ± 4
	60	173 ± 14	74 ± 4
	165	106 ± 4	55 ± 4
0.6	44	189 ± 27	64 ± 0
	60	232 ± 9	72 ± 11
	165	155 ± 23	58 ± 9

4.9 Corrosion

Mesh #60 was further examined for possible corrosion by running the MECs for 15 cycles and observing the stability of the performance at an applied voltage of 0.9 V. The initial gas production and current densities increased slightly over the first four cycles and stabilized for the next 10 cycles. A slight decrease in gas production (below 30 mL) was observed from the 14th cycle. At the end of 15th cycle, methane concentration of 5 ± 1 % was measured while the current didn't drop, which indicated that the decrease in gas production was not due to the mesh corrosion but rather to hydrogen conversion to methane. (Figure **4-13**).

The surfaces of new and used SS mesh (20 days after use) were observed using SEM (Figure **4-14**). No major surface corrosion was observed under 5 × magnifications (A & B). The larger magnification in the photo indicated minor surface texture changes as seen in D. The metal composition by SEM-EDS (Table **4-8**) shows small differences before and after use. The composition was unchanged in chromium, iron and nickel, indicating stable metals composition for the observed catalytic performance of SS 304 mesh (76, 77).

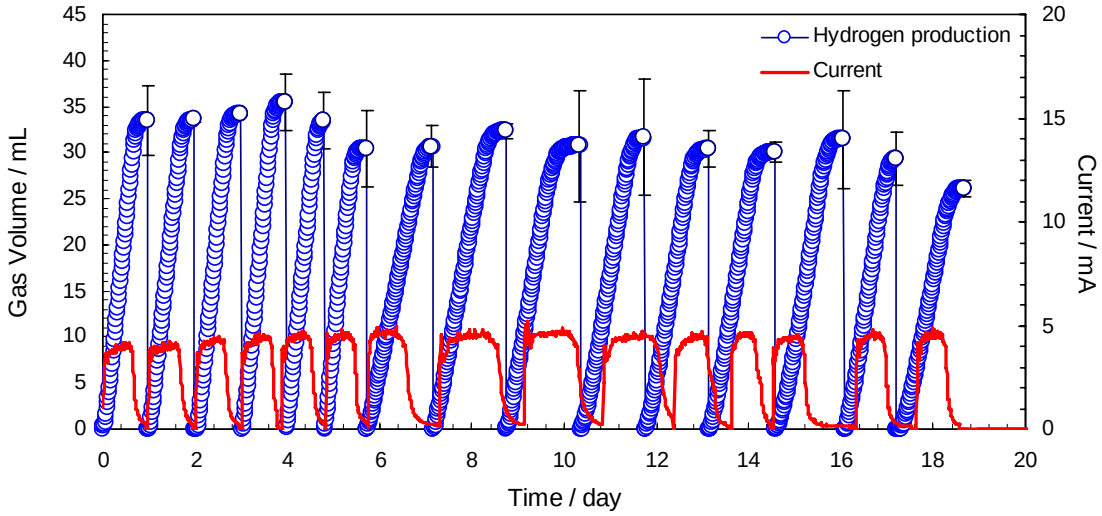

Figure 4-13: Total gas and current production versus time with SS mesh #60 cathode at E_{ap} = 0.9 V.

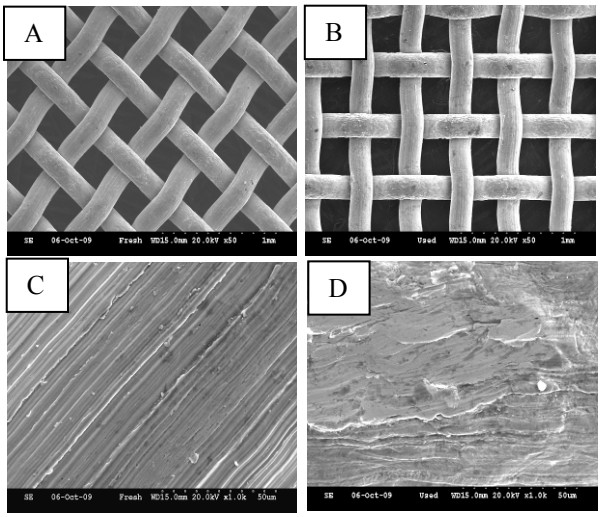

Figure 4-14: SEM image of SS mesh #60 before (A and C) and after 20 day use (B and D) as cathode in MEC. (A) and (B) are at 5 × magnification and (C) and (D) are at 1,000 × magnification.

Table 4-8: Metal composition of SS mesh #60 by SEM-EDS before and after 1 month of use in MEC as cathode. Table 3-9: Metal composition of SS mesh #60 by SEM-EDS before and after 1 month of use in MEC as cathode.

Weight percent / %	Fresh	Used
C	0.12	0.083 ± 0.015
Si	0.11	0.29 ± 0.046
Cr	18.39	18.61± 0.71
Fe	72.76	72.65 ± 0.11
Ni	8.62	7.97 ± 0.41

4.10 Use of SS mesh as Cathode and Carbon Mesh as Anode in a Bottle MEC

The startup time of electrodes using a plastic separator (SEP) or without a separator (EMP) was 2 days, compared to 10 days for electrodes containing a glass fiber separator (GF). The currents obtained during the first cycle for SEP and GF were around 4 mA. An increase in current was observed in EMP reactors on the third cycle (Figure **4-15**). The comparison of current generation between two reactor configurations was made on the basis of the average maximum volumetric current densities I_v and current densities calculated on the basis of cathode area I_a (Table **4-9**). EMP electrodes with close electrode (1.5 mm) spacing and no separator showed a current improvement of 1 $A \cdot m^{-2}$.

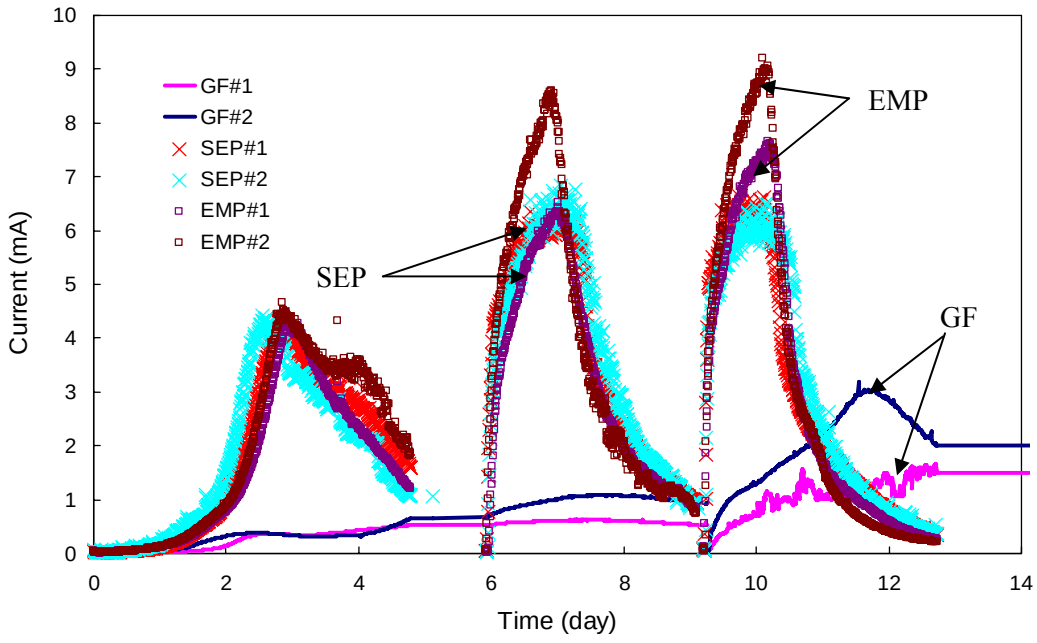

Figure 4-15: Current output for bottle MECs with different electrode constructions.

Table 4-9: Comparison of the maximum volumetric current densities and superficial current densities for two types of electrode construction in different reactors.

E_{ap} = 0.9 V	Single-cell cubic reactor (30ml, 7 cm^2)	Bottle reactor (110ml, 8 cm^2)
I_v / A m^{-3}	188 ± 19	67 ± 5
I_a / A m^{-2}	8.1 ± 0.8	9.2 ± 0.7

Chapter 5

Discussion

5.1 Effect of Mesh Characteristic on Hydrogen Evolution Rate

The electrode surface areas, bubble retention on the electrode are main influence factors on cathode overpotential and hydrogen evolution rates. It is generally accepted that a larger surface area to volume ratio of a catalyst results in higher catalytic performance. Dense mesh wire produced a large active surface area (66 m^2/m^3 for mesh #60 and 65 m^2/m^3 for mesh #30). Mesh #60, which had the densest wire and largest active surface area, required the lowest overpotential (–0.63 V in LSV test) and achieved the highest current densities in MECs (281 A/m^3 at 1.2 V, 188 A/m^3 at 0.9 V and 90 A/m^3 at 0.6 V).

Very small mesh pore sizes did not appear to be useful for hydrogen gas production likely due to entrapment of small bubbles, resulting in an increase in cathode overpotential. For example, mesh #165 produced the highest overpotential (–0.72 V in LSV tests), which had a relatively large active surface area 61 m^2/m^3 but a smaller pore size (0.011 cm), than mesh #60 (0.023 cm). The cathode potential of #165 in MECs was substantially lower than #60 mesh, especially at higher currents when bubble entrapment was more obvious. (Figure **4-7**, **4-8**).

The large pore size was a main factor for increasing hydrogen production in the medium current range in LSV tests (Figure **4-2.B**). Adhering bubbles lead to blockage of a fraction of the wire surface, resulting in a catalytically inactive surface, and a decrease in the current density (78). In the medium current range, there was an evident drop in V_h, an indicator of less effective catalytic performance (65), for most mesh except those with very large pore sizes (Table **5-1**). The smaller the pore size, the more V_h declined. When bubbles grew to the size needed to break-off the mesh (break-off diameter), bubble coverage was the highest and gas evolution efficiency

was low. The break-off diameter varies with liquid-gas contact angle, surface tension (79), current density, and was affected by mesh pore size in tests here. There is a longer residence time of the bubbles on the mesh with smaller pore sizes (Figure **4-7**) because the break-off diameter was more easily reached on smaller pore size mesh.

Table 5-1: Slope of the applied voltage (V_h) in low, medium and high current range (shown in Figure 3-9) for different meshes.

Linear Range	Mesh number	V_h/ mA V^{-1}
Line 1 (6~10 mA)	44	81
	60	82
	165	89
Line 2 (15~20 mA)	44	83
	60	46
	165	25
Line 3 (30~35 mA)	44	171
	60	264
	165	290

The bubble coverage is estimated to be less than 5% on MEC cathodes based on an empirical equation correlating the bubble coverage Θ and superficial current density on horizontally placed flat electrode in stagnant electrolyte as (78):

$$\Theta = 0.023\left(\frac{I/A}{\mathrm{A\,m^{-2}}}\right)^{0.23} \tag{5-1}$$

where the typical current range is less than 10 mA in MECs. I visually observed in MECs that bubbles only formed on a small portion of the mesh and then quickly departed the mesh surface. Thus, the active surface area was still the main factor in MEC operation conditions tested here even though a larger pore size was helpful for current generation, making up for area deficiency at high currents. Mesh #44 with larger pore size (0.04 cm) but smaller active surface area (41 m^2/m^3) than mesh #60 (0.02 cm, 66 m^2/m^3) produced only 2–3% less current densities at higher currents (1.2 V applied), but 13% less current at a lower current (0.6 V applied). Thus, there is a

point where further increases in pore size requires a reduction in the total active surface area, and thus very large pore sizes may not be helpful at low current densities.

At very high current densities, however, bubbles evolved more quickly from the surface creating shear that helped to remove bubbles. This suggests that stirring or creating shear flow near the surface of the electrodes would affect hydrogen evolution rate, to an extent dependent on the mesh characteristics.

5.2 Limiting Factor on Current Generation

The maximum current was limited by the performance of the biofilm on the anode at higher applied voltages (≥ 1.1 V) because it resulted in more positive anode potentials (> –0.1 V). Lee et al. (75) showed that more negative anode potentials help improve MEC performance, consistent with that observed here that more positive anode potentials were detrimental to MEC.-

Lower current densities at low applied voltages were likely to be a result of less effective catalytic activity of the SS mesh. As the cathode voltage was approaching the minimum required voltage for hydrogen production, the slope of the cathode voltage (V_h) decreased substantially (Table **5-2,** calculated based on Figure **4-7**). The same trend was observed in LSV results. Thus, 0.9 to 1.1 V would be the optimum applied voltage to produce the most efficient hydrogen evolution using SS mesh.

Table 5-2: Slope of the cathode voltage (V_h) of flat SS and SS meshes in different linear current range in MECs.

Applied Voltage / V	Cathode Voltage / V vs. SHE	Cathode	V_h / mA V^{-1}	R^2
0.6–0.7	-0.87 – -0.95	Flat SS	3.74	1
	-0.85 – -0.94	Mesh #60	4.15	1
0.7–0.9	-0.95 – -1.11	Flat SS	13.51	0.977
	-0.94 – -1.10	Mesh #60	11.75	0.999
0.9–1.1	-1.11 – -1.27	Flat SS	28.26	0.873
	-1.10 – -1.22	Mesh #60	21.88	0.998

5.3 Efficiency

The relatively lower coulombic efficiency at higher voltage (E_{ap}> 1 V, E_{anode} > –0.2 V) implied that an anode potential more positive than –0.2 V may not be favorable for electrochemically active bacteria. This findings corresponds to Chae et al's work (48), which suggested that the shift in the anode potential could inhibit the electrochemically active bacteria growing at anode potentials at –0.2 to –0.28 V, resulting in a decreased CE. Coulombic efficiences greater than 100% occurred at lower applied voltages here. Lee et al. (80) proposed that H_2 would be oxidized by anode bacteria once acetate was not detectable and produce current. Thus, in this study, the longer batch time at lower applied voltage allowed the recycle of H_2 between the cathode and the anodes and increased CE over 100%.

The cathodic hydrogen recovery of SS mesh reached a maximum value (close to 100%) at an applied voltage of >1.0 V, and then the hydrogen recovery declined with applied voltage. The microbiological loss of hydrogen to methane was likely the main reason for lower hydrogen recovery. The total hydrogen recovery loss for SS mesh #60 from the highest value to lowest was 25–35%. The higher methane concentrations of mesh #60 after long time use at 0.6 V (C_{CH4} = 4.6 ± 1.1 %) contributed most to hydrogen recovery losses, while the other H_2 loss was likely to be a result of various factors. Lee et al. (80) showed a decline in r_{cat} when $\boldsymbol{r_{CE}}$ increased to over 100%, regardless of negligible CH_4 formation. The less effective catalytic activity of the SS mesh at lower applied voltages and longer batch times could be the potential causes as well.

5.4 Outlook for Using SS Mesh as a Cathode

Among the different materials examined here, SS mesh #60 exhibited the best results in terms of current densities, hydrogen and energy recoveries. The current density of 90 ± 7 $A \cdot m^{-3}$

(applied voltage =0.6 V) with 66 m^2/m^3 specific surface area per reactor volume, however, was half that obtained with a high surface area SS brush (810 m^2/m^3) (68) or using carbon cloth with Pt (Pt/CC) cathodes (20). This suggests that comparable current densities to SS brushes or Pt/CC at low applied voltage could be achieved by using multiple SS mesh cathodes. The SS mesh is very light (1.05 kg/ m^2) and flexible enough to be built into any reactor configuration, which could allow for closer placement next to the anode and thus lower ohmic losses (24). Based on these findings, it should be possible to create a new MEC electrode design based on combing low cost heat-treated carbon mesh anodes and SS mesh cathodes placed only 1.5 mm apart. Preliminary experiments have shown the enhancement of current density per cathode area (Table 4-9).

Using low cost SS mesh will greatly reduce capital cost and makes a promising step forward to building the large scale reactors. The cost of SS mesh cathode in 30ml reactor is $0.004, compared to $0.03 for the half SS brush cathode and $0.15 for the Pt on the Pt/C cathode (81, 82). The overall electrode material (including ca. $25/$m^2$ for carbon mesh anode (60) and $90/$m^2$ for SS mesh#60 (www.mcmaster.com)) costs only 3 to 5 % of the traditional material using carbon cloth and platinum.

Chapter 6

Conclusions

Stainless steel mesh, as a more scalable and low-cost cathode was first examined in MECs. The results obtained demonstrated that:

1. SS woven mesh performed better than expanded mesh as a catalyst for hydrogen evolution.

2. The largest active surface area measured by CV reached specific area of 78 m^2/m^3 (SS mesh #120), which is three times the active surface area of a flat sheet.

3. An optimum size range existed for different current ranges and bubble coverages. Mesh wire size was the dominant factor of hydrogen evolution rate at low currents (< 10 mA) and small bubble coverages. The wire diameter of 0.02–0.03 cm was most beneficial to the hydrogen evolution rate. Mesh pore size was dominant at medium currents (10–40 mA) and high bubble coverages. Large pore size (> 0.04 cm) mesh allowed for more efficient gas evolution. At high currents (40–100 mA), mesh wire diameter and pore size were of fairly equal in importance to current generation.

4. In MECs with SS mesh as a cathode, the current range was smaller than 10 mA with low bubble coverage. SS mesh #60 with dense wire and medium pore sizes (active surface area: 66 m^2/m^3) performed the best in terms of current density, maximum hydrogen production rate and hydrogen recovery. (I_v = 188 ± 19 A m^{-3}, Q_{H2} = 2.1 ± 0.3 m^3H_2/m^3-d, r_{cat} = 99 % at E_{ap} = 0.9 V).

5. Higher applied voltages (>1.1 V, anode potential > –0.1 V) limited anode performance and current production rate. Low applied voltages (< 0.9 V) reduced the catalytic activity and hydrogen recovery. The optimum applied voltage was 0.9 V in respect to high hydrogen recovery and overall energy efficiency.

6. SS mesh did not show any evidence of corrosion over time in MEC tests conducted here.

Chapter 7

Future Work

There are still challenges to be addressed for improving the performance of the system:

1. It would be interesting to try multiple layers of mesh or corrugated mesh to increase cathode surface areas and improve current densities. This work showed that the larger active surface area was the most critical factor at low current for improving current generation so multiple cathodes could be more practical for a possible scale up of the system.
2. New reactor designs would be helpful to improve current generation. The new designs would require large cathode surface areas and closer electrode space. The optimum electrode spacing and the necessity of using separator between electrodes should be further tested.
3. Methane generation needs to be reduced, as does electron recycling to improve hydrogen yield and recovery.

Appendix A

Mesh Surface Area Calculation Example

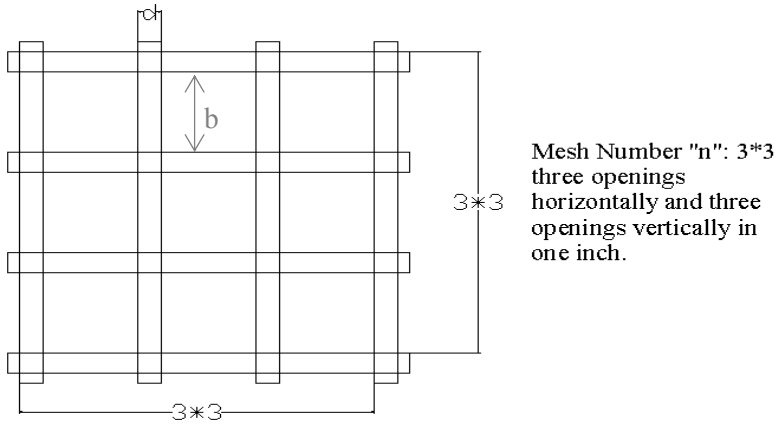

Figure A-1: SS 304 woven mesh configuration, where *n* is mesh size, *d* is wire diameter and *b* is pore size.

Within 1 inch × 1 inch mesh grid, the surface area includes $2n(n+1)$ cylinder segments (diameter = *d*, length = *b*) and $(n+1)^2$ junction areas (diameter = *d*, length = d). The cylinder segment area is:

$$S_0 = \pi d \times b \quad \text{in}^2 / \text{in}^2$$

Assume the junction area loss at one point is ¼ of the two cross-over small cylinders, which leads to the area of one junction as:

$$S_J = \frac{3}{2}\pi d^2 \quad \text{in}^2 / \text{in}^2$$

Real surface area per inch^2 is

$$S = S_0 \times 2n(n+1) + S_J \times (n+1)^2$$

$$S = 2\pi b d\, n(n+1) + \frac{3}{2}\pi\, d^2 (n+1)^2 \quad \text{in}^2 / \text{in}^2 \text{ (or cm}^2 / \text{cm}^2)$$

Example: 30 mesh (n=30, d=0.012 in, b=0.012 in)

$$S = 2\pi b\, d\, n(n+1) + \frac{3}{2}\pi\ d^2(n+1)^2 \quad \text{in}^2 / \text{in}^2 \text{ (or cm}^2 / \text{cm}^2\text{)}$$

$$S = 2\pi \times 0.0305 \times 0.0305 \times 30 \times (30+1) + \frac{3}{2}\pi\ 0.0305^2(30+1)^2$$

$$= 1.49 \text{ in}^2 / \text{in}^2 \text{ (or cm}^2 / \text{cm}^2\text{)}$$

Specific area per 7 cm^2 cathode: $S \times 7 = 10.45 \text{ cm}^2$

Specific area per reactor volume: $S\ / 30\,\text{ml} = 0.35 \text{ cm}^2 / \text{cm}^3 = 0.35 \times 100 = 35 \text{ m}^2/\text{m}^3$

Appendix B

LSV Scan Results for Different Size Mesh

Each mesh was performed LSV scans three times as illustrated in Figure **B-1**. At the beginning of each scan, a new mesh replaced the used one. The results showed reasonable reproducibility. Thus the third cycle of LSV scan was used for analysis (Figure **B-2)** (step size between each data point = 0.1 mV). The current at different cathode potential was shown in Table **B-1**.

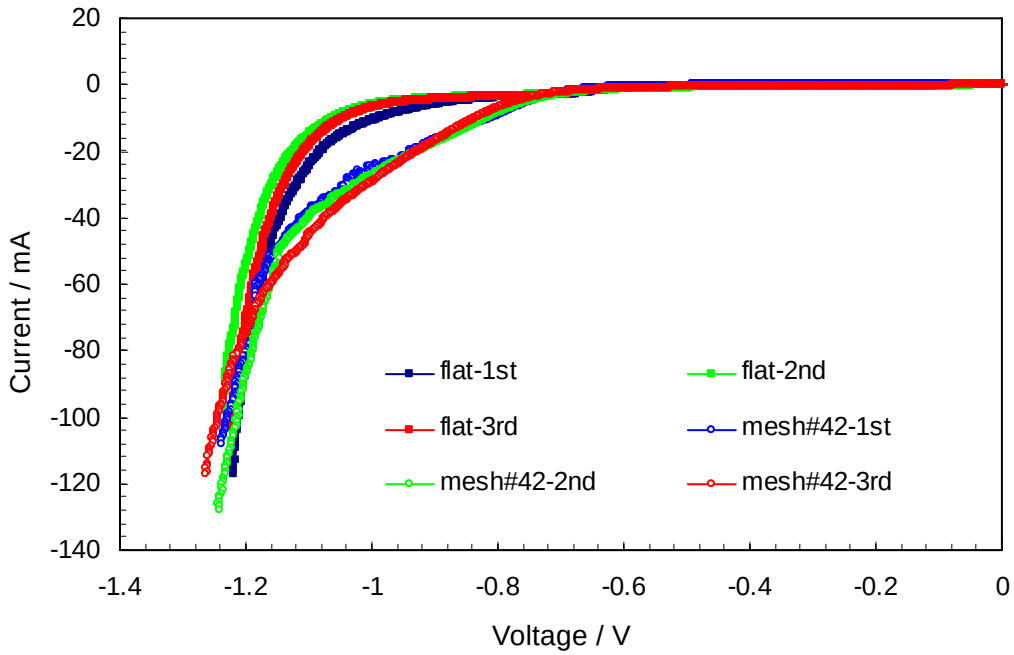

Figure B-1: Examples of three time LSV scans for flat SS and mesh#42.

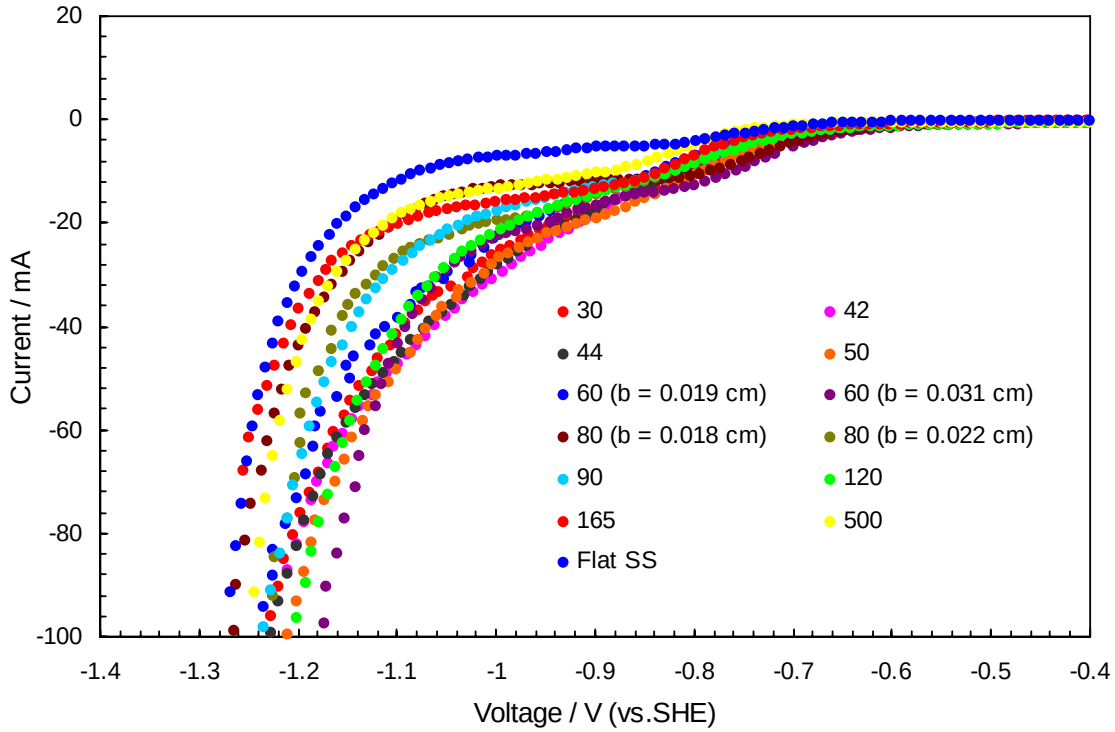

Figure B-2: Currents of different SS mesh at different cathode potential.

Table B-1: Current taken from LSV results (Figure **B-2**) of different SS mesh at different cathode potential (vs. SHE).

Cathode potential / V	–0.6	–0.7	–0.8	–0.9	–1.0	–1.1	–1.2
Mesh number	**Current / mA**						
30	1.32	3.82	10.60	17.20	26.50	41.40	76.10
42	1.10	2.50	7.66	18.60	30.90	46.80	80.10
44	1.20	3.00	9.60	18.00	28.80	45.90	81.20
50	1.23	3.59	11.30	19.50	28.20	48.70	91.00
60	1.03	2.40	7.55	14.60	23.00	38.10	75.50
60	1.62	5.68	12.90	16.80	23.20	43.40	119.00
80	1.20	2.94	8.82	14.90	19.80	26.60	63.40
80	1.19	2.50	7.77	15.70	21.50	27.60	53.10
90	1.28	3.36	10.30	16.80	22.60	32.30	72.30
120	1.30	3.08	9.01	14.70	22.40	39.70	94.80
165	0.90	2.03	7.45	13.70	16.20	20.50	36.30
500	0.71	1.14	4.78	10.48	14.64	22.05	55.28

Appendix C

Original 3D Graph of Current Distribution

(A)

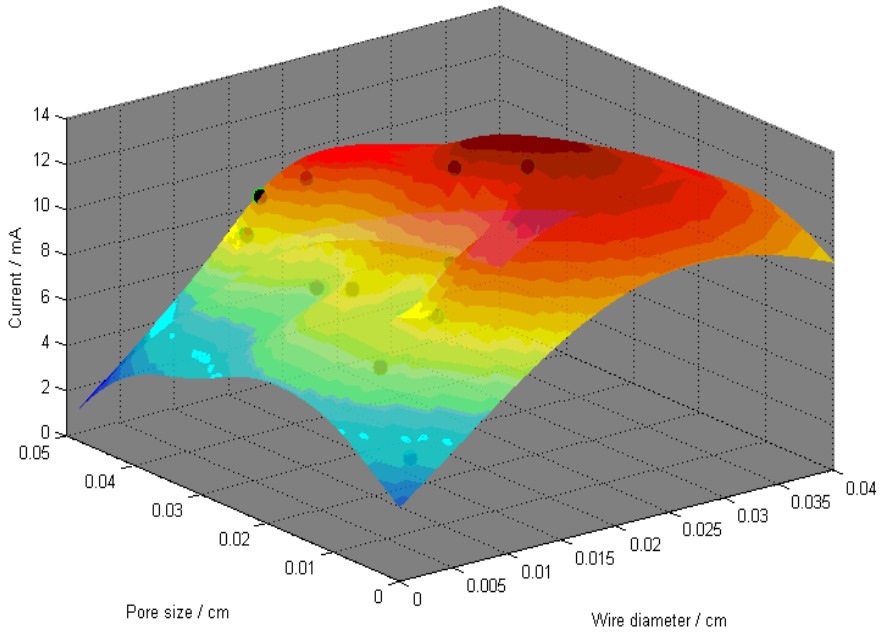

(B)

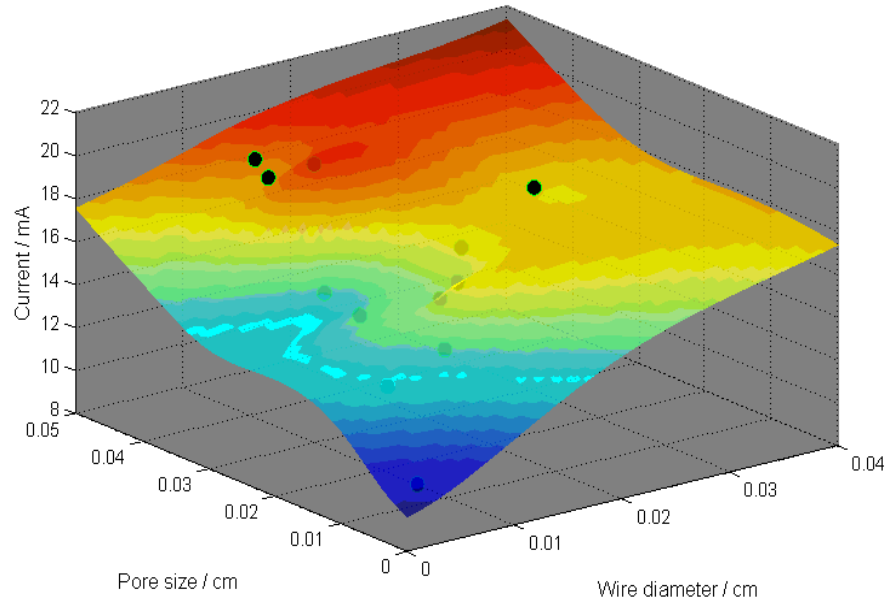

(C)

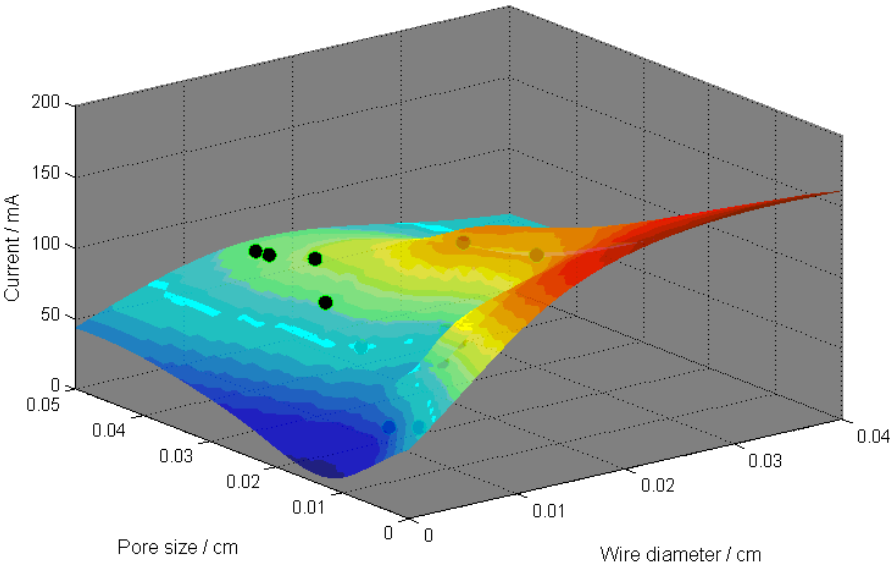

Figure C-1: Original current magnitude distribution in a three-dimensional space at low current (A), medium current (B) and large current (C).

REFERENCES

1. Martinot, E. *Renewables 2007 global status report* REN21: 2007.
2. *BP Statistical Review of World Energy*; June 2009.
3. A statement of the problem in capsule form. http://planetforlife.com/
4. MacKenzie; James, J., *The Keys to the Car.* World Resources: Baltimore, 1994.
5. Oxtoby, D. W., *Principles of Modern Chemistry (5th ed.)*. Thomson Brooks/Cole.: 2002.
6. Kotay, S. M.; Das, D., Biohydrogen as a renewable energy resource - Prospects and potentials. *International Journal of Hydrogen Energy* **2008,** *33*, (1), 258-263.
7. Levin, D. B.; Pitt, L.; Love, M., Biohydrogen production: prospects and limitations to practical application. *International Journal of Hydrogen Energy* **2004,** *29*, (2), 173-185.
8. Logan, B. E., Extracting hydrogen electricity from renewable resources. *Environmental Science & Technology* **2004,** *38*, (9), 160a-167a.
9. Grant, P. M., Hydrogen lifts off - with a heavy load - The dream of clean, usable energy needs to reflect practical reality. *Nature* **2003,** *424*, (6945), 129-130.
10. Gross, R.; Leach, M.; Bauen, A., Progress in renewable energy. *Environment International* **2003,** *29*, (1), 105-122.
11. Ivy, J. *Summary of electrolytic hydrogen production: milestone completion report*; National Renewable Energy Laboratory (NREL): 2004.
12. Hallenbeck, P. C.; Benemann, J. R., Biological hydrogen production; fundamentals and limiting processes. *International Journal of Hydrogen Energy* **2002,** *27*, (11-12), 1185-1193.
13. Hawkes, F. R.; Hussy, I.; Kyazze, G.; Dinsdale, R.; Hawkes, D. L., Continuous dark fermentative hydrogen production by mesophilic microflora: Principles and progress. *International Journal of Hydrogen Energy* **2007,** *32*, (2), 172-184.
14. Ust'ak, S.; Havrland, B.; Munoz, J. O. J.; Fernandez, E. C.; Lachman, J., Experimental verification of various methods for biological hydrogen production. *International Journal of Hydrogen Energy* **2007,** *32*, (12), 1736-1741.
15. Kapdan, I. K.; Kargi, F., Bio-hydrogen production from waste materials. *Enzyme and Microbial Technology* **2006,** *38*, (5), 569-582.
16. Manish, S.; Banerjee, R., Comparison of biohydrogen production processes. *International Journal of Hydrogen Energy* **2008,** *33*, (1), 279-286.
17. Liu, H.; Grot, S.; Logan, B. E., Electrochemically assisted microbial production of hydrogen from acetate. *Environmental Science & Technology* **2005,** *39*, (11), 4317-4320.
18. Logan, B. E., *Microbial Fuel Cells*. John Wiley & Son, Inc: 2008.
19. Miyake, J.; Miyake, M.; Asada, Y., Biotechnological hydrogen production: research for efficient light energy conversion. *Journal of Biotechnology* **1999,** *70*, (1-3), 89-101.
20. Call, D.; Logan, B. E., Hydrogen production in a single chamber microbial electrolysis cell lacking a membrane. *Environmental Science & Technology* **2008,** *42*, (9), 3401-3406.
21. Nath, K.; Das, D., Hydrogen from biomass. *Current Science* **2003,** *85*, (3), 265-271.
22. Kim, I. S.; Hwang, M. H.; Jang, N. J.; Hyun, S. H.; Lee, S. T., Effect of low pH on the activity of hydrogen utilizing methanogen in bio-hydrogen process. *International Journal of Hydrogen Energy* **2004,** *29*, (11), 1133-1140.

23. Logan, B. E.; Call, D.; Cheng, S.; Hamelers, H. V. M.; Sleutels, T. H. J. A.; Jeremiasse, A. W.; Rozendal, R. A., Microbial Electrolysis Cells for High Yield Hydrogen Gas Production from Organic Matter. *Environmental Science & Technology* **2008,** *42*, (23), 8630-8640.
24. Rozendal, R. A.; Hamelers, H. V. M.; Rabaey, K.; Keller, J.; Buisman, C. J. N., Towards practical implementation of bioelectrochemical wastewater treatment. *Trends in Biotechnology* **2008,** *26*, (8), 450-459.
25. Call, D. F.; Merrill, M. D.; Logan, B. E., High Surface Area Stainless Steel Brushes as Cathodes in Microbial Electrolysis Cells. *Environmental Science & Technology* **2009,** *43*, (6), 2179-2183.
26. Call, D. Hydrogen production in a microbial electrolysis cell lacking a membrane. Penn State University, 2008.
27. Rozendal, R. A.; Hamelers, H. V. M.; Euverink, G. J. W.; Metz, S. J.; Buisman, C. J. N. Process for producing hydrogen. 2005.
28. Rozendal, R. A.; Hamelers, H. V. M.; Euverink, G. J. W.; Metz, S. J.; Buisman, C. J. N., Principle and perspectives of hydrogen production through biocatalyzed electrolysis. *International Journal of Hydrogen Energy* **2006,** *31*, (12), 1632-1640.
29. Cheng, S.; Logan, B. E., Sustainable and efficient biohydrogen production via electrohydrogenesis. *Proceedings of the National Academy of Sciences of the United States of America* **2007,** *104*, (47), 18871-18873.
30. Rozendal, R. A. Wageningen University, 2007.
31. Logan, B. E.; Grot, S. A bioelectrochemically assisted microbial reactor (BEAMR) that generates hydrogen gas. 60/588,022, 2005.
32. Logan, B. E.; Hamelers, B.; Rozendal, R. A.; Schrorder, U.; Keller, J.; Freguia, S.; Aelterman, P.; Verstraete, W.; Rabaey, K., Microbial fuel cells: Methodology and technology. *Environmental Science & Technology* **2006,** *40*, (17), 5181-5192.
33. Liu, H.; Logan, B. E., Electricity generation using an air-cathode single chamber microbial fuel cell in the presence and absence of a proton exchange membrane. *Environmental Science & Technology* **2004,** *38*, (14), 4040-4046.
34. Liu, H.; Ramnarayanan, R.; Logan, B. E., Production of electricity during wastewater treatment using a single chamber microbial fuel cell. *Environmental Science & Technology* **2004,** *38*, (7), 2281-2285.
35. Cheng, H.; Scott, K.; Ramshaw, C., Intensification of water electrolysis in a centrifugal field. *Journal of the Electrochemical Society* **2002,** *149*, (11), D172-D177.
36. Oh, S.; Min, B.; Logan, B. E., Cathode performance as a factor in electricity generation in microbial fuel cells. *Environmental Science & Technology* **2004,** *38*, (18), 4900-4904.
37. Kim, J. R.; Min, B.; Logan, B. E., Evaluation of procedures to acclimate a microbial fuel cell for electricity production. *Applied Microbiology and Biotechnology* **2005,** *68*, (1), 23-30.
38. Logan, B. E.; Oh, S. E.; Kim, I. S.; Van Ginkel, S., Biological hydrogen production measured in batch anaerobic respirometers. *Environmental Science & Technology* **2002,** *36*, (11), 2530-2535.
39. Cheng, S. A.; Liu, H.; Logan, B. E., Optimization of air cathode used in one-chamber microbial fuel cells. *Abstracts of Papers of the American Chemical Society* **2004,** *228*, U639-U639.
40. Logan, B. E.; Murano, C.; Scott, K.; Gray, N. D.; Head, I. M., Electricity generation from cysteine in a microbial fuel cell. *Water Research* **2005,** *39*, (5), 942-952.
41. Min, B. Perchlorate remediation using packed-bed bioreactors and electricity generation in microbial fuel cells (MFCs). Dissertation, Penn State University, Univeristy Park, 2005.
42. Bond, D. R.; Holmes, D. E.; Tender, L. M.; Lovley, D. R., Electrode-reducing microorganisms that harvest energy from marine sediments. *Science* **2002,** *295*, (5554), 483-485.

43. Bond, D. R.; Lovley, D. R., Electricity production by Geobacter sulfurreducens attached to electrodes. *Applied and Environmental Microbiology* **2003,** *69*, (3), 1548-1555.
44. Rabaey, K.; Lissens, G.; Siciliano, S. D.; Verstraete, W., A microbial fuel cell capable of converting glucose to electricity at high rate and efficiency. *Biotechnology Letters* **2003,** *25*, (18), 1531-1535.
45. Kim, H. J.; Park, H. S.; Hyun, M. S.; Chang, I. S.; Kim, M.; Kim, B. H., A mediator-less microbial fuel cell using a metal reducing bacterium, Shewanella putrefaciense. *Enzyme and Microbial Technology* **2002,** *30*, (2), 145-152.
46. Park, H. S.; Kim, B. H.; Kim, H. S.; Kim, H. J.; Kim, G. T.; Kim, M.; Chang, I. S.; Park, Y. K.; Chang, H. I., A novel electrochemically active and Fe(III)-reducing bacterium phylogenetically related to Clostridium butyricum isolated from a microbial fuel cell. *Anaerobe* **2001,** *7*, (6), 297-306.
47. Logan, B. E.; Regan, J. M., Electricity-producing bacterial communities in microbial fuel cells. *Trends in Microbiology* **2006,** *14*, (12), 512-518.
48. Chae, K. J.; Choi, M. J.; Lee, J.; Ajayi, F. F.; Kim, I. S., Biohydrogen production via biocatalyzed electrolysis in acetate-fed bioelectrochemical cells and microbial community analysis. *International Journal of Hydrogen Energy* **2008,** *33*, (19), 5184-5192.
49. Ditzig, J.; Liu, H.; Logan, B. E., Production of hydrogen from domestic wastewater using a bioelectrochemically assisted microbial reactor (BEAMR). *International Journal of Hydrogen Energy* **2007,** *32*, (13), 2296-2304.
50. Rozendal, R. A.; Hamelers, H. V. M.; Molenkmp, R. J.; Buisman, J. N., Performance of single chamber biocatalyzed electrolysis with different types of ion exchange membranes. *Water Research* **2007,** *41*, (9), 1984-1994.
51. Liu, W. Z.; Wang, A. J.; Ren, N. Q.; Zhao, X. Y.; Liu, L. H.; Yu, Z. G.; Lee, D. J., Electrochemically assisted biohydrogen production from acetate. *Energy & Fuels* **2008,** *22*, (1), 159-163.
52. Rozendal, R. A.; Jeremiasse, A. W.; Hamelers, H. V. M.; Buisman, C. J. N., Hydrogen production with a microbial biocathode. *Environmental Science & Technology* **2008,** *42*, (2), 629-634.
53. Tartakovsky, B.; Manuel, M. F.; Neburchilov, V.; Wang, H.; Guiot, S. R., Biocatalyzed hydrogen production in a continuous flow microbial fuel cell with a gas phase cathode. *Journal of Power Sources* **2008,** *182*, (1), 291-297.
54. Hu, H. Q.; Fan, Y. Z.; Liu, H., Hydrogen production using single-chamber membrane-free microbial electrolysis cells. *Water Research* **2008,** *42*, (15), 4172-4178.
55. Wang, A. J.; Liu, W. Z.; Cheng, S. A.; Xing, D. F.; Zhou, J. H.; Logan, B. E., Source of methane and methods to control its formation in single chamber microbial electrolysis cells. *International Journal of Hydrogen Energy* **2009,** *34*, (9), 3653-3658.
56. Lay, J. J.; Lee, Y. J.; Noike, T., Feasibility of biological hydrogen production from organic fraction of municipal solid waste. *Water Research* **1999,** *33*, (11), 2579-2586.
57. Rabaey, K.; Boon, N.; Siciliano, S. D.; Verhaege, M.; Verstraete, W., Biofuel cells select for microbial consortia that self-mediate electron transfer. *Applied and Environmental Microbiology* **2004,** *70*, (9), 5373-5382.
58. Rabaey, K.; Clauwaert, P.; Aelterman, P.; Verstraete, W., Tubular microbial fuel cells for efficient electricity generation. *Environmental Science & Technology* **2005,** *39*, (20), 8077-8082.
59. Logan, B.; Cheng, S.; Watson, V.; Estadt, G., Graphite fiber brush anodes for increased power production in air-cathode microbial fuel cells. *Environmental Science & Technology* **2007,** *41*, (9), 3341-3346.

60. Wang, X.; Cheng, S. A.; Feng, Y. J.; Merrill, M. D.; Saito, T.; Logan, B. E., Use of Carbon Mesh Anodes and the Effect of Different Pretreatment Methods on Power Production in Microbial Fuel Cells. *Environmental Science & Technology* **2009,** *43*, (17), 6870-6874.
61. Liu, H.; Cheng, S. A.; Logan, B. E., Power generation in fed-batch microbial fuel cells as a function of ionic strength, temperature, and reactor configuration. *Environmental Science & Technology* **2005,** *39*, (14), 5488-5493.
62. Cheng, S.; Liu, H.; Logan, B. E., Increased power generation in a continuous flow MFC with advective flow through the porous anode and reduced electrode spacing. *Environmental Science & Technology* **2006,** *40*, (7), 2426-2432.
63. Freguia, S.; Rabaey, K.; Yuan, Z.; Keller, J., Non-catalyzed cathodic oxygen reduction at graphite granules in microbial fuel cells. *Electrochimica Acta* **2007,** *53*, (2), 598-603.
64. Clauwaert, P.; Toledo, R.; Van der Ha, D.; Crab, R.; Verstraete, W.; Hu, H.; Udert, K. M.; Rabaey, K., Combining biocatalyzed electrolysis with anaerobic digestion. *Water Science and Technology* **2008,** *57*, (4), 575-579.
65. Cheng, S. A.; Logan, B. E., Evaluation of catalysts and membranes for high yield biohydrogen production via electrohydrogenesis in microbial electrolysis cells (MECs). *Water Science and Technology* **2008,** *58*, (4), 853-857.
66. Selembo, P. A.; Merrill, M. D.; Logan, B. E., The use of stainless steel and nickel alloys as low-cost cathodes in microbial electrolysis cells. *Journal of Power Sources* **2009,** *190*, (2), 271-278.
67. Munoz, L. D.; Benjamin, E.; Luc, E.; Julien, R.; Regine, B.; Alain, B., Combing phosphate species and stainless steel cathode to enhance hydrogen evolution in microbial electrolysis cell (MEC). *Electrochemistry Communications* **2010,** *12*, 183-186.
68. Harnisch, F.; Schroder, U.; Quaas, M.; Scholz, F., Electrocatalytic and corrosion behaviour of tungsten carbide in near-neutral pH electrolytes. *Applied Catalysis B-Environmental* **2009,** *87*, (1-2), 63-69.
69. ASTM, Document number A 959-07. Standard guide for specifying harmonized standard grade compositions for wrought stainless steels. Table 1. Chemical Composition Limits, %. **October 4, 2008**.
70. Bard, A. J.; Faulkner, L. R., *Electrochemical Methods: Fundamentals and Application*. Wiley: New York, 1982.
71. Cheng, S. A.; Logan, B. E., Ammonia treatment of carbon cloth anodes to enhance power generation of microbial fuel cells. *Electrochemistry Communications* **2007,** *9*, (3), 492-496.
72. Zinder, S. H.; Anguish, T.; Cardwell, S. C., Selective-Inhibition by 2-Bromoethanesulfonate of Methanogenesis from Acetate in a Thermophilic Anaerobic Digester. *Applied and Environmental Microbiology* **1984,** *47*, (6), 1343-1345.
73. Zhang, X. Y.; Cheng, S. A.; Wang, X.; Huang, X.; Logan, B. E., Separator Characteristics for Increasing Performance of Microbial Fuel Cells. *Environmental Science & Technology* **2009,** *43*, (21), 8456-8461.
74. Sandwell, D. T., Biharmonic Spline Interpolation of Geos-3 and Seasat Altimeter Data. *Geophysical Research Letters* **1987,** *14*, (2), 139-142.
75. Lee, H. S.; Torres, C. I.; Rittmann, B. E., Effects of Substrate Diffusion and Anode Potential on Kinetic Parameters for Anode-Respiring Bacteria. *Environmental Science & Technology* **2009,** *43*, (19), 7571-7577.
76. Marcelo, D.; Dell'Era, A., Economical electrolyser solution. *International Journal of Hydrogen Energy* **2008,** *33*, (12), 3041-3044.
77. Olivares-Ramirez, J. M.; Campos-Cornelio, M. L.; Godinez, J. U.; Borja-Arco, E.; Castellanos, R. H., Studies on the hydrogen evolution reaction on different stainless steels. *International Journal of Hydrogen Energy* **2007,** *32*, (15), 3170-3173.

78. Vogt, H.; Balzer, R. J., The bubble coverage of gas-evolving electrodes in stagnant electrolytes. *Electrochimica Acta* **2005,** *50*, (10), 2073-2079.
79. Stephan, K., *Heat transfer in condensation and boiling*. Springer: Berlin, 1992.
80. Lee, H. S.; Torres, C. I.; Parameswaran, P.; Rittmann, B. E., Fate of H-2 in an Upflow Single-Chamber Microbial Electrolysis Cell Using a Metal-Catalyst-Free Cathode. *Environmental Science & Technology* **2009,** *43*, (20), 7971-7976.
81. MEPS., World Stainless Steel Prices. In.
82. Kitco., 24h platinum spot chart. In.